



# ANCF analysis of the crude oil sloshing in railroad vehicle systems

Emanuele Grossi, Ahmed A. Shabana\*

Department of Mechanical and Industrial Engineering, University of Illinois at Chicago, Chicago, IL 60607, USA



## ARTICLE INFO

### Article history:

Received 14 March 2018

Received in revised form 12 June 2018

Accepted 14 June 2018

Available online 26 July 2018

Handling Editor: Erasmo Carrera

### Keywords:

Crude oil

Railroad vehicle dynamics

Non-Newtonian fluid

Liquid sloshing

Absolute nodal coordinate formulation

Multibody system dynamics

## ABSTRACT

With the increase in *crude oil* rail transportation, accurate modelling of non-Newtonian crude oil rheological properties and the corresponding nonlinear sloshing effects becomes necessary in order to establish safety and operation guidelines. In this investigation, nonlinear continuum-based crude oil constitutive models are used in a total Lagrangian formulation to study the effect of the sloshing on railroad vehicle dynamics and stability. In particular, the Oldroyd constitutive model is employed to capture the non-Newtonian characteristics of three different crude oil types; classified as *light*, *medium*, and *heavy*. The crude oil complex deformation shapes are captured using the finite element (FE) absolute nodal coordinate formulation (ANCF). The FE continuum-based liquid sloshing formulation is systematically integrated with a fully nonlinear multibody system (MBS) railroad vehicle algorithm that allows for wheel/rail separation. A general penalty contact approach is developed to allow for studying the effect of sloshing suppression devices such as bulkheads. Different braking scenarios, including electronically controlled pneumatic (ECP) braking are considered to study the effect of crude oil sloshing on the train longitudinal stability. The ECP braking computer simulations show that increasing the crude oil viscosity can lead to approximately 30% reduction in the maximum coupler force compared to the light oil case. It is observed that the coupler force response to the sloshing excitations as the result of ECP braking reaches steady state faster as the viscosity increases. Furthermore, installing the bulkheads in tank cars can lead to a 70% reduction in the maximum coupler force and more uniform distribution of the normal contact forces to the front and rear wheels. The effect of crude oil rheological properties on the centrifugal forces during curve negotiation is also evaluated. The curve negotiation results show that the increase in crude oil density is responsible for exacerbating train lateral instability effects, thus the risk of vehicle roll over, especially when the train travels at a speed higher than the balance speed.

© 2018 Elsevier Ltd. All rights reserved.

## 1. Introduction

While the derailments of trains transporting hazardous materials (HAZMAT) have been reduced in the past few years, the economic and environmental damage resulting from the HAZMAT rail transportation remains a serious daily threat, particularly with the increasing demand for crude oil transportation. In order to reduce such a damage, more credible safety

\* Corresponding author.

E-mail addresses: [egrossi20@uic.edu](mailto:egrossi20@uic.edu) (E. Grossi), [shabana@uic.edu](mailto:shabana@uic.edu) (A.A. Shabana).

and operation guidelines as well as design standards must be developed based on accurate and scientifically convincing physics-based modeling techniques. Minimizing HAZMAT-transportation accidents can be achieved by developing computer simulation approaches that accurately account for the continuum-based crude oil rheological material properties, allow optimizing the tank car designs, test rail equipment durability, and examine new braking system concepts. The Federal Railroad Administration (FRA) reported that the safety of HAZMAT rail transportation in the United States has significantly improved over the past fifty years [1]. However, the increasing demand of crude oil and other HAZMAT transportation has resulted in several deadly and environmentally damaging rail accidents. Several derailment accidents during the past two decades involved the release of hazardous materials; examples of which are the train derailments in North Dakota [2] and Ontario [3], and the train collisions in Texas [4] and South Carolina [5]. Among the most recent accidents, a train carrying crude oil derailed in the Chicago area with an estimated leak of 45,000 gallons in the summer of 2017 [6]. In order to avoid accidents involving HAZMAT transportation, the railroad industry is actively conducting multiple research projects to improve railroad vehicle designs. The Volpe National Transportation System Center is performing studies on the structural integrity of railroad tank cars transporting hazardous materials [7]. A new project called the Next Generation Rail Tank Car (NGRTC) is a collaborative research and development effort sponsored by multiple companies with the aim of improving tank car design [8]. Nonetheless, understanding the liquid sloshing phenomenon is necessary in order to better identify the cause of and potentially prevent future HAZMAT transportation derailments.

## 2. Background and scope of the investigation

This investigation is focused on integrating continuum-based crude oil rheological constitutive laws, such as the *Oldroyd constitutive model*, with computational MBS algorithms for the study of the sloshing effect on railroad vehicle dynamics. Using the physics-based modeling approach developed in this study, one can distinguish between different crude oil viscosity properties and their effect on the rail vehicle motion and stability. The development of such continuum-based sloshing models is necessary in order to have alternatives for the simplified non-physics-based discrete mass-spring system models often used in the analysis of liquid sloshing, as will be discussed in this section. This section also provides background materials that explain the motivation for this study and defines the scope and specific contributions of this investigation.

### 2.1. Liquid sloshing and classical vibration problems

Sloshing is not a typical mechanical vibration problem because the motion of fluids is not influenced by the restoring forces that produce and sustain solid oscillations. A typical vibration problem requires the existence of two basic elements; *inertia* and *restoring force elements*. While damping can significantly influence mechanical vibrations, damping is not a necessary element for discrete-mass vibrations to exist. The restoring elastic force element does not enter into the definition of the liquid sloshing phenomenon or its mathematical description. Fluids do not have restoring forces; the fluid motion is mainly influenced by the viscous forces often defined using the Navier-Stokes equations. Because stiffness coefficients cannot be determined from viscosity coefficients using any parameter identification method, discrete mass-spring system sloshing models are not physics-based. A fluid can flow out of a container or a tank car, as in the case with deadly, costly, and environmentally damaging accidents, because of the lack of restoring forces that can be mathematically defined using a strain energy function.

The fluid/container interaction is often modeled using a penalty force approach to enforce *unilateral constraints*. Such unilateral constraint forces cannot be derived from a fluid strain-energy function, which cannot be justified using physics principles. Because fluid forces are viscous forces defined using dissipation functions and not strain energy functions, the use of costly experiments to validate non-physics-based discrete mass-spring sloshing models needs to be justified. For this reason, the focus of this paper will be on the development of new continuum- and physics-based crude oil sloshing models that allow for using appropriate and realistic viscosity coefficients to study the effect of the oil motion on the rail vehicle dynamics and stability.

### 2.2. Experimental testing and simulation models

To better understand the dynamic loads applied to railroad tank cars, wheels, and couplers; it is important to develop liquid sloshing formulations, which account for the nonlinear fluid/structure interaction effects, which occur during the complex railroad operating conditions. The liquid oscillations resulting from the interaction with the tank walls result in uneven loading even in normal service conditions and represent a potential source of instability, derailment, and structural failure. In order to reduce the severe sloshing oscillations of viscous fluids, tank cars can be fully loaded. This solution, however, may lead to a significant increase of the axle load and normal wheel/rail contact forces, especially when high-density fluids like crude oils are transported. Many railroad accident investigations are mainly focused on fatigue analysis, collision dynamics, and structural response. In order to conduct these investigations successfully and produce reliable results, an accurate load spectrum must be defined. The load spectrum can be produced experimentally by means of advanced microprocessors and sensors mounted on the rail car equipment. Nonetheless, experimental testing is extremely expensive, prone to human error, highly sensitive to weather conditions, and often show large data variations within the same set of measurements. Reliance on experimental data can be reduced only if complex high-fidelity MBS railroad vehicle models with

significant details including liquid sloshing effects are developed. Furthermore, as previously mentioned, costly experiments designed to validate non-physics-based models must have a strong justification.

### 2.3. Crude oil sloshing

Several liquid sloshing formulations have been developed in the literature to account for the effect of fluid/structure interaction. One approach approximates the liquid sloshing behavior using equivalent mechanical models, such as spring-mass-damper and pendulum systems [9–12]. These models are based on a simple implementation, consider the effects of static and dynamic pressure of the fluid, and can be used to obtain real-time simulations. However, the reduction in simulation time comes at the expense of a significant decrease in numerical accuracy and the generality of the approach. Discrete inertia models cannot be used to model the fluid free surface and cannot capture the change in fluid inertia resulting from large deformations, which is critical in the study of liquid sloshing oscillations. The introduction of springs in discrete inertia models is equivalent to assuming elastic restoring forces in the fluid, which contradicts the basic fluid dynamic principles, as previously explained. The definition of the stiffness and damping coefficients of a fluid-like discrete inertia model is a trial-and-error process rather than directly using the known fluid viscous properties. Furthermore, the discrete inertia models cannot capture correctly the tank geometry or the highly nonlinear dynamic effects of non-Newtonian fluids, whose motion is governed by constitutive relationships, which are more general.

Other continuum-based techniques can be mainly categorized under the Lagrangian or Eulerian approaches. Lagrangian methods accurately predict the fluid free surface but tend to be less numerically accurate in the case of large mesh distortions. On the other hand, Eulerian schemes are best suited for investigating turbulent flows but require additional efforts to capture the free surface shape. In the past decades, mesh-free Lagrangian techniques have also been introduced, such as smoothed particle hydrodynamics (SPH). Mesh-free methods can describe complex multi-phase flows including turbulence, but are computationally very expensive [13,14]. A continuum-based total Lagrangian non-incremental liquid sloshing formulation based on the finite element (FE) absolute nodal coordinate formulation (ANCF) was proposed by Wei et al. [15]. This formulation can be systematically integrated with complex MBS vehicle models such as tanker truck and railroad vehicle models [16,17]. The main advantages, limitations, and range of applicability of this method are discussed in detail in Ref. [67].

The analysis of sloshing phenomena using the ANCF total Lagrangian formulation has been limited until now to the case of simple Newtonian fluids. The increasing demand of crude oil transportation by rail makes the analysis of crude oil sloshing an important safety and environmental issue that must be addressed in order to improve railroad design standards and safety and operation guidelines. Most crude oils exhibit non-Newtonian behavior including *thixotropy*, *pseudoplasticity*, and *waxing* at low temperatures. A common misconception is that these phenomena occur only at Arctic temperatures; in reality, even crude oils produced in warm regions like Australia and central Africa present very high non-Newtonian transition temperatures [18]. *Waxy crude oils* are among the most complex non-Newtonian crude oils produced around the world. These types of oil represent around 20% of the world petroleum reserves and 80% of crude oil production in China [19]. Below the *wax appearance temperature* (WAT), the wax content in the oil solidifies and imparts strong nonlinear rheological characteristics to the fluid dynamics, including a yield stress [20]. The complex rheological behavior of crude oil necessitates the development of algorithms that allow for investigating the sloshing effects of highly viscous non-Newtonian fluids on railroad vehicle dynamics and stability.

### 2.4. Scope and contributions of this investigation

In this paper, the continuum-based total Lagrangian FE/ANCF liquid sloshing formulation is generalized to the analysis of non-Newtonian fluids and is systematically integrated with complex MBS railroad-vehicle models. The analysis of both free and constrained crude oil sloshing oscillations inside railroad tank cars is considered. The study of less restricted fluid oscillations is important because many tank cars in various countries still lack bulkheads and baffles. However, in order to address the most recent technological developments in the area of sloshing suppression devices, a robust MBS algorithm must be designed to allow for capturing the effect of the relative motion and interaction between the fluids and anti-sloshing devices. This paper makes the following specific contributions:

- 1) Four **non-Newtonian constitutive models** that allow for investigating nonlinear crude oil sloshing effects are presented and the corresponding ANCF generalized viscous forces are derived. The development of different non-Newtonian ANCF fluid constitutive models allows for extending the use of existing ANCF continuum-based total Lagrangian liquid sloshing formulation to the analysis of most crude oils currently transported by rail and highway.
- 2) The effect of installing liquid **sloshing suppression devices** on railroad vehicle dynamics are examined using the newly developed continuum-based fluid models. A penalty contact algorithm is developed to model the interaction between the ANCF continuum-based fluid mesh and a tank with bulkheads. The ability to install sloshing suppression devices in MBS tanker train virtual models is necessary in order to allow for realistic simulation of detailed railroad vehicle models, most of which include bulkheads or baffles.
- 3) The ANCF fluid model is systematically integrated with two complex MBS railroad-vehicle models. Numerical simulations are performed using the general-purpose MBS software **SIGMA/SAMS** (Systematic Integration of Geometric Modeling and

Analysis for the Simulation of Articulated Mechanical Systems) to study the effect of crude **oil rheological properties** on railroad vehicle dynamics. Three different crude oil types; classified as *light*, *medium*, and *heavy*, are analyzed. The sloshing effects generated by different crude oil types on the train *coupler force* are investigated in the case of braking scenarios, including **ECP braking**, and in the case of curve negotiations.

This paper is organized as follows. In Section 3, the most popular crude oil constitutive models used in the petroleum industry are described. In Section 4, the ANCF non-Newtonian generalized viscous forces are derived for four different crude oil constitutive models and the formulation of the ANCF inertia and centrifugal forces is explained. Sections 5 and 6 present the formulation of the bulkhead penalty-contact model and the MBS governing equations of motion, respectively. In Section 7, the three-dimensional wheel/rail contact model used in this investigation is briefly discussed; this contact formulation allows for the wheel/rail separation. Section 8 presents analysis of the numerical results obtained in this study.

### 3. ANCF fluid constitutive models

In this section, the general Newtonian and non-Newtonian ANCF constitutive models applicable to both low- and high-viscous fluids are described. The use of absolute position and gradient vectors as nodal coordinates allows the ANCF displacement field to describe accurately arbitrarily large displacements and rotations, as well as complex fluid geometry [21]. The fluid is assumed incompressible and the effect of temperature is neglected. The kinetic and kinematic ANCF equations can describe the fluid behavior in three different configurations, namely the straight, stress-free curved reference, and current configurations, shown in Fig. 1. The use of these configurations allows for describing systematically the initially curved fluid geometry defined by the tank surface. Let  $V$ ,  $V_0$ , and  $v$  be the fluid volumes in the straight, curved reference, and current configurations, respectively, and  $\mathbf{x}$ ,  $\mathbf{X}$ , and  $\mathbf{r}$  be the corresponding position vectors of an arbitrary point on the fluid. The position vector of an arbitrary point on an ANCF element  $j$  can be defined in the curved reference and current configurations, respectively, as  $\mathbf{X}^j = [x^j \ y^j \ z^j]^T = \mathbf{S}^j \mathbf{e}_0^j$  and  $\mathbf{r}^j = \mathbf{S}^j \mathbf{e}^j$ , where  $\mathbf{S}^j$  is the ANCF shape function matrix,  $\mathbf{e}_0^j$  and  $\mathbf{e}^j$  are the element nodal coordinates in the curved reference and current configurations, respectively [21]. The volumes in the curved reference and current configurations are related by the determinant of the matrix of position vector gradients  $\mathbf{J}^j$  as  $dV^j = \mathbf{J}^j dV_0^j$ , where  $\mathbf{J}^j = \partial \mathbf{r}^j / \partial \mathbf{X}^j$ . The integration over the initially curved reference configuration can be simplified by introducing a straight reference configuration, which can be related to the curved reference configuration using the relationship  $dV_0^j = \mathbf{J}_0^j dV^j$ , where  $\mathbf{J}_0^j = \partial \mathbf{X}^j / \partial \mathbf{x}^j$  is a constant Jacobian matrix. The current and straight configurations are related by  $dV^j = \mathbf{J}_e^j dV^j$ , where  $\mathbf{J}_e^j$  is the determinant of the matrix  $\mathbf{J}_e^j = \partial \mathbf{r}^j / \partial \mathbf{x}^j$ . Therefore, the matrix of position vector gradients that enter into the formulation of the Green-Lagrange strain tensor can be written as  $\mathbf{J}^j = \partial \mathbf{r}^j / \partial \mathbf{X}^j = (\partial \mathbf{r}^j / \partial \mathbf{x}^j)(\partial \mathbf{x}^j / \partial \mathbf{X}^j) = \mathbf{J}_e^j \mathbf{J}_0^{j-1}$ .

#### 3.1. Non-Newtonian crude oil constitutive models

The rheological behavior of fluids is classified depending on the relationship between the shear stress and shear rate; a fluid is defined as *Newtonian* if the relationship is linear. The Cauchy stress tensor for an isotropic Newtonian fluid can be expressed as  $\boldsymbol{\sigma} = [-p + \lambda \text{tr}(\mathbf{D})]\mathbf{I} + 2\mu\mathbf{D}$ , where  $p$  is the fluid hydrostatic pressure defined as  $p = -(1/3)\text{tr}(\boldsymbol{\sigma})$ ,  $\mathbf{D} = (1/2)[\partial \mathbf{v} / \partial \mathbf{r} + (\partial \mathbf{v} / \partial \mathbf{r})^T]$  is the rate of deformation tensor,  $\lambda$  is Lame's constant,  $\mu$  is the coefficient of dynamic viscosity,  $\mathbf{v}$  is the velocity vector,  $\partial \mathbf{v} / \partial \mathbf{r} = \mathbf{L}$  is the matrix of velocity gradients, and  $\text{tr}$  is the trace of a matrix. If the relationship between shear stress and shear rate is not linear, then the fluid is defined as *non-Newtonian*. Above room temperature, most crude oils behave as Newtonian fluids with low viscosity and a single phase. However, most crude oils that contain high molecular weight compounds such as paraffin crystals undergo significant changes in their rheological properties as the temperature decreases

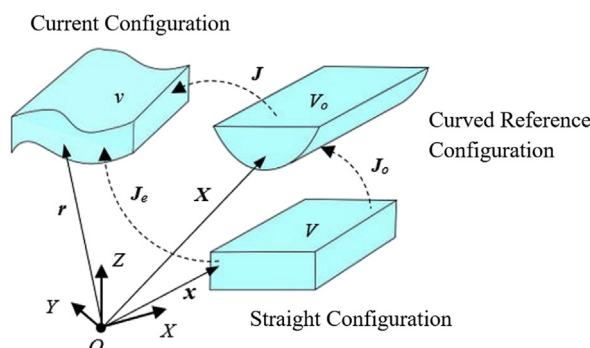


Fig. 1. Straight, reference, and current configurations.

[22]. The formation of interlocking structures and crystallization mechanisms inside the fluid are typical phenomena that occur in *waxy crude oils*, a class of crude oils whose production and transportation has significantly increased over the last 20 years, and which currently represent 80% of petroleum reserves in China [23]. As the temperature drops below the *wax appearance temperature* (WAT), the fluid viscosity increases sharply and a gel-like structure forms, which presents an initial elastic response until the shear stress exceeds the yield stress, leading to the structure breakdown and reappearance of a shear flow [20]. The fluid yield stress is reached due to the particular spatial orientation of the solid crystals formed below the WAT. The yield stress represents the transition from the elastic solid to the viscous liquid states [24].

The effect of thermal and shear history, the temperature- and shear-dependence of yield stress and viscosity, and the existence of WAT make the analysis of Non-Newtonian crude oils a challenging task. Significant work has been devoted in the literature to develop constitutive models that describe the complex rheological behavior of waxy crude oils. The development of the first visco-plastic constitutive models with yield stress started in the beginning of the twentieth century with the work of Schrödoff [25], followed by the work of Bingham in 1922 [26], who proposed a one-dimensional version of the Maxwell viscoelastic model assuming a rigid fluid behavior below the yield stress. In 1926, Herschel and Bulkley [27] proposed a visco-plastic constitutive model, where the dynamic viscosity coefficient is defined as a power-law function of the shear rate. The Bingham constitutive laws have been formulated in the three-dimensional case by Hohenemser and Prager in 1932 [28]. In 1947, Oldroyd proposed three-dimensional constitutive equations for a Bingham solid assuming a linear Hookean elastic behavior in the elastic state [29]. Among the more recent studies, Saramito developed in 2007 a fluid constitutive equation that considers the fluid as a Kelvin-Vogit viscoelastic solid before yielding and as an Oldroyd viscoelastic fluid after yielding [30]. In 2009, Saramito combined the Oldroyd viscoelastic model and the Herschel-Bulkley visco-plastic model in a new three-dimensional form that satisfies the second law of thermodynamics [31]. Constitutive models such as Bingham, Casson, Herschel-Bulkley, and Oldroyd are not appropriate to describe fluid transient regimes and are referred to in the literature as *time-independent models*. Several authors attempted to describe the thixotropic transient behavior of crude oils by adding to the fluid constitutive equations the time derivative of a scalar parameter  $\lambda_f(t)$ , which accounts for the fluid microstructure [32–37]. Other authors further coupled the fluid thixotropic behavior with time-dependent yield stress effects [38–41]. Despite the several assumptions and limitations, the most common rheological constitutive models of yield stress fluids used in the petroleum industry until today are the ones developed by Bingham, Oldroyd, Herschel and Bulkley, and Casson. The fluid constitutive models for the four cases are briefly presented in their three-dimensional form in the following subsections.

### 3.2. Bingham constitutive model

The Bingham constitutive model can be written in a tensor form as:

$$\begin{aligned} \sigma &= 2\mu D + \tau_0 D / \|D\| && \text{if } \|\sigma\| \geq \tau_0 \\ D &= \mathbf{0} && \text{if } \|\sigma\| < \tau_0 \end{aligned} \quad (1)$$

where  $\tau_0$  is the yield stress,  $\mu$  is the dynamic viscosity,  $D$  is the rate of deformation tensor, and  $\|\sigma\| = \sqrt{(1/2)(\sigma : \sigma)}$  is the Euclidian norm of the Cauchy stress tensor [23]. If the norm of the stress tensor  $\|\sigma\|$  is greater than  $\tau_0$ , the crude oil behaves like an incompressible, isotropic, visco-plastic fluid. However, if the yield stress is not exceeded, the rate of deformation tensor  $D$  is the null matrix and the fluid behaves as a solid-like rigid body. This model can be extended to the non-isothermal case by allowing  $\mu$  and  $\tau_0$  to be functions of temperature [23]. Frigaard et al. [18] introduced a Bingham model to study the isothermal weakly-compressible visco-plastic flow of waxy crude oils.

### 3.3. Herschel-Bulkley constitutive model

In contrast to the constant viscosity assumption of the Bingham constitutive model, in Herschel-Bulkley fluids, the viscosity follows a power-law behavior. The three-dimensional Herschel-Bulkley fluid constitutive equation can be written as

$$\begin{aligned} \sigma &= 2\mu D \|D\|^{n-1} + \tau_0 D / \|D\| && \text{if } \|\sigma\| \geq \tau_0 \\ D &= \mathbf{0} && \text{if } \|\sigma\| < \tau_0 \end{aligned} \quad (2)$$

where  $n$  is the power-law index. According to the Herschel-Bulkley constitutive model, the fluid behavior is nonlinear after yielding. If  $n < 1$  the fluid assumes a shear thinning behavior, that is, the viscosity decreases as the shear rate increases, if  $n > 1$  the behavior is defined as shear thickening and the viscosity increases with the shear rate. In case  $n = 1$ , the Herschel-Bulkley constitutive model reduces to the Bingham model.

### 3.4. Oldroyd constitutive model

Oldroyd proposed fluid constitutive equations based on the Bingham model, but relaxed the rigid body assumption when the yield stress is not exceeded. The fluid rigid body assumption is replaced with a perfect Hookean solid behavior, where the stress field depends linearly on the strain. The Oldroyd constitutive model is written as

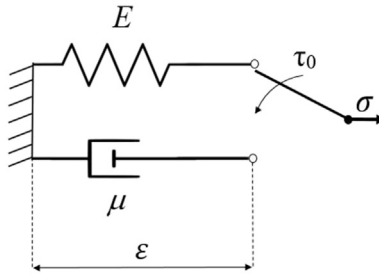


Fig. 2. One-dimensional Oldroyd constitutive model.

$$\left. \begin{array}{ll} \sigma = 2\mu D + \tau_0 D / \|D\| & \text{if } \|\sigma\| \geq \tau_0 \\ \sigma = E : \epsilon & \text{if } \|\sigma\| < \tau_0 \end{array} \right\} \quad (3)$$

where  $E$  is the matrix of elastic coefficients. The Oldroyd constitutive model is represented schematically for the one-dimensional case in Fig. 2. The switch activates either the linear elastic Hookean behavior or the viscous behavior, depending on the magnitude of the norm of the Cauchy stress tensor relative to the yield stress.

### 3.5. Casson constitutive model

The Casson constitutive model depends on two parameters ( $\mu$  and  $\tau_0$ ), similar to the Bingham model. This constitutive model was originally introduced to study lithographic varnishes, but its use has been extended to the analysis of other non-Newtonian fluids like crude oils [42]. The Casson constitutive model is written in its three-dimensional form as

$$\left. \begin{array}{ll} \sigma = 2\mu D (1 + 2\sqrt{\tau_0 / \|D\|}) + \tau_0 D / \|D\| & \text{if } \|\sigma\| \geq \tau_0 \\ \sigma = \mathbf{0} & \text{if } \|\sigma\| < \tau_0 \end{array} \right\} \quad (4)$$

The four rheological crude oil constitutive models discussed in this section can be systematically implemented in a continuum-physics-based ANCF approach to study the effect of sloshing on vehicle dynamics and stability. The Oldroyd constitutive model will be given a special attention in this investigation because such a constitutive model does not simplify the fluid state to the rigid body case when the yield stress is not exceeded.

## 4. ANCF viscous and inertia forces

In this section, the formulation of the generalized inertia and non-Newtonian viscous forces associated with the ANCF nodal coordinates is discussed. The fluid generalized viscous forces are formulated for each crude oil constitutive model presented in Section 3. While in the case of the ANCF elements the expression of the inertia forces is simple, the viscous forces assume a more complex form. The ANCF crude oil viscous force formulation allows for arbitrary fluid displacements including finite rotations.

### 4.1. Non-Newtonian crude oil viscous forces

The crude oil constitutive models described in Section 3 are formulated using the Cauchy stress tensor  $\sigma$  defined in the current configuration. While this stress tensor represents the true stress, it cannot be used directly in the case of the large deformation with the Green-Lagrange strain tensor  $\epsilon$  which is associated with the reference configuration. The Green-Lagrange strain tensor is used with the second Piola-Kirchhoff stress tensor  $\sigma_{P2}$ . For a finite element  $j$  of the fluid mesh, the virtual work of the fluid viscous forces can be written in the current and reference configurations as

$$\delta W_v^j = - \int_{V^j} \sigma^j : (\delta \mathbf{J}^j) (\mathbf{J}^j)^{-1} dV^j = - \int_{V_0^j} \sigma_{P2}^j : \delta \epsilon^j dV_0^j \quad (5)$$

where superscript  $j$  refers to the element number,  $\epsilon^j = (\mathbf{J}^T \mathbf{J}^j - \mathbf{I})/2$  is the Green-Lagrange strain tensor, and  $\sigma_{P2}^j = \mathbf{J}^j (\mathbf{J}^j)^{-1} \sigma^j (\mathbf{J}^j)^{-1T}$  is the second Piola-Kirchhoff stress tensor. By substituting the expression of the Cauchy stress tensor defined by the crude oil constitutive models into the equation for the second Piola-Kirchhoff stress tensor, the following general equation can be written:

$$\sigma_{p2}^j = a^j j^j (\mathbf{J}^j)^{-1} \mathbf{D}^j (\mathbf{J}^j)^{-1T} \quad (6)$$

where  $a^j$  is a scalar parameter, defined for each ANCF element  $j$ , which depends on the Non-Newtonian constitutive model used. Because  $\mathbf{D}^j = (\mathbf{J}^j)^{-1T} \dot{\mathbf{e}}^j (\mathbf{J}^j)^{-1}$ , one has

$$\begin{aligned} \delta W_v^j &= - \int_{V_0^j} a^j j^j (\mathbf{J}^j)^{-1} (\mathbf{J}^j)^{-1T} \dot{\mathbf{e}}^j (\mathbf{J}^j)^{-1} (\mathbf{J}^j)^{-1T} : \delta \mathbf{e}^j dV_0^j \\ &= - \int_{V_0^j} a^j j^j (\mathbf{C}_r^j)^{-1} \dot{\mathbf{e}}^j (\mathbf{C}_r^j)^{-1} : \delta \mathbf{e}^j dV_0^j \end{aligned} \quad (7)$$

where  $\mathbf{C}_r^j = (\mathbf{J}^j)^T \mathbf{J}^j$  is the right Cauchy-Green deformation tensor. Using the virtual change in the strain tensor  $\delta \mathbf{e}^j = (\partial \mathbf{e}^j / \partial \mathbf{e}^j) \delta \mathbf{e}^j$  in Equation (5) where  $\mathbf{e}^j$  is the vector of the element nodal coordinates, the generalized viscous forces associated with the ANCF nodal coordinates can be written for the Bingham and Oldroyd, Herschel-Bulkley, and Casson constitutive models, respectively, as:

$$\left. \begin{aligned} \mathbf{Q}_v^j &= - \int_{V_0^j} \left( 2\mu + \frac{\tau_0}{\|\mathbf{D}^j\|} \right) j^j \left[ (\mathbf{C}_r^j)^{-1} \dot{\mathbf{e}}^j (\mathbf{C}_r^j)^{-1} \right] : \frac{\partial \mathbf{e}^j}{\partial \mathbf{e}^j} dV_0^j \\ \mathbf{Q}_v^j &= - \int_{V_0^j} \left( 2\mu \|\mathbf{D}^j\|^{n-1} + \frac{\tau_0}{\|\mathbf{D}^j\|} \right) j^j \left[ (\mathbf{C}_r^j)^{-1} \dot{\mathbf{e}}^j (\mathbf{C}_r^j)^{-1} \right] : \frac{\partial \mathbf{e}^j}{\partial \mathbf{e}^j} dV_0^j \\ \mathbf{Q}_v^j &= - \int_{V_0^j} \left[ 2\mu \left( 1 + 2 \sqrt{\frac{\tau_0}{\|\mathbf{D}^j\|}} \right) + \frac{\tau_0}{\|\mathbf{D}^j\|} \right] j^j \left[ (\mathbf{C}_r^j)^{-1} \dot{\mathbf{e}}^j (\mathbf{C}_r^j)^{-1} \right] : \frac{\partial \mathbf{e}^j}{\partial \mathbf{e}^j} dV_0^j \end{aligned} \right\} \quad (8)$$

The crude oil incompressibility condition can be imposed using the technique of *Lagrange multipliers* or the *penalty method*. The former method introduces additional algebraic equations and constraint forces to the MBS dynamic equations [21] and requires, in general, a more sophisticated numerical solution procedure. The penalty method does not require introducing algebraic constraint equations; however, excessively large penalty coefficients increase the stiffness of the system and may lead to numerical problems. In this paper, the penalty method is used to impose the incompressibility condition. The relationship between the fluid volumes in the current and initially curved reference configurations can be written as  $dv = J dV_0$ . In case of an incompressible fluid, the constraint  $j^j = 1$  for a finite element  $j$  is enforced by introducing the penalty strain energy function  $U_{IC}^j = (1/2)k_{IC}^j(j^j - 1)^2$ , where  $k_{IC}^j$  is a problem-dependent penalty coefficient which must be carefully selected to satisfy the incompressibility constraint to within acceptable tolerance. The vector of generalized volumetric penalty forces associated with the ANCF nodal coordinates for an element  $j$  can be defined as  $\mathbf{Q}_{IC}^j = \partial U_{IC}^j / \partial \mathbf{e}^j = k_{IC}^j(j^j - 1)(\partial j^j / \partial \mathbf{e}^j)$ . The incompressibility constraint at the velocity level  $j^j = 0$  is enforced using the vector of generalized forces  $\mathbf{Q}_{TD}^j = \partial U_{TD}^j / \partial \mathbf{e}^j = c_{TD}^j(j^j / \partial \mathbf{e}^j)$ , where  $U_{TD}^j = (1/2)c_{TD}^j(j^j)^2$  is a dissipation function and  $c_{TD}^j$  is a penalty damping coefficient. In the three-dimensional analysis,  $j^j = \mathbf{r}_X^j \cdot (\mathbf{r}_Y^j \times \mathbf{r}_Z^j) = \mathbf{r}_Y^j \cdot (\mathbf{r}_Z^j \times \mathbf{r}_X^j) = \mathbf{r}_Z^j \cdot (\mathbf{r}_X^j \times \mathbf{r}_Y^j)$ , where subscripts X, Y, and Z refer to partial differentiation of the position vector  $\mathbf{r}$  with respect to the subscript parameters. One can also show that  $(\partial j^j / \partial \mathbf{e}^j) = (\partial j^j / \partial \mathbf{e}^j) = \mathbf{S}_X^T(\mathbf{r}_Y^j \times \mathbf{r}_Z^j) + \mathbf{S}_Y^T(\mathbf{r}_Z^j \times \mathbf{r}_X^j) + \mathbf{S}_Z^T(\mathbf{r}_X^j \times \mathbf{r}_Y^j)$ . The vector of generalized penalty forces associated with the nodal coordinates of the ANCF element  $j$  can then be written as  $\mathbf{Q}_P^j = \mathbf{Q}_{IC}^j + \mathbf{Q}_{TD}^j$ .

#### 4.2. ANCF generalized inertia forces

One of the main advantages of the total Lagrangian continuum-based ANCF formulation is the ability to account for the effect of the fluid distributed inertia using a constant inertia matrix and a non-incremental solution procedure regardless of the amount of displacement and rotation of the finite element. The crude oil distributed inertia plays an important role in the study of the nonlinear sloshing forces. The formulation of the ANCF inertia forces requires evaluating the fluid acceleration vector, which for an ANCF element  $j$  can be written simply as  $\mathbf{a}^j = \mathbf{S}^j \dot{\mathbf{e}}^j$ , where  $\mathbf{S}^j$  is the element shape function matrix. The virtual work of the inertia forces can be defined in the current configuration as  $\delta W_i^j = \int_{V_0^j} \rho^j \mathbf{a}^j \cdot \delta \mathbf{r}^j dV_0^j$ , where the virtual change in the fluid position vector can be written as  $\delta \mathbf{r}^j = \mathbf{S}^j \delta \mathbf{e}^j$ . Using these two equations, the virtual work of the inertia forces can be written in the reference curved configuration for an ANCF element  $j$  as

$$\delta W_i^j = \left\{ \mathbf{e}^{j^T} \int_{V_0^j} \rho_0^j \mathbf{S}^{j^T} \mathbf{S}^j dV_0^j \right\} \delta \mathbf{e}^j = \left\{ \ddot{\mathbf{e}}^{j^T} \mathbf{M}^j \right\} \delta \mathbf{e}^j = \mathbf{Q}_i^{j^T} \delta \mathbf{e}^j \quad (9)$$

where  $\rho_0^j = \rho^j j$  is the mass density in the reference configuration,  $\rho^j$  is the mass density in the current configuration,  $\mathbf{M}^j = \int_{V_0^j} \rho_0^j \mathbf{S}^{j^T} \mathbf{S}^j dV_0^j$  is the constant symmetric ANCF mass matrix, and  $\mathbf{Q}_i^j = \mathbf{M}^j \ddot{\mathbf{e}}^j$  is the vector of generalized fluid inertia forces associated with the ANCF nodal coordinates. The unique constant mass matrix feature of the ANCF elements simplifies significantly the fluid governing equations since it leads to zero centrifugal and Coriolis forces.

#### 4.3. Outward inertia forces

In the case of liquid sloshing, the outward inertia force during curve negotiations has an expression that differs from the centrifugal inertia force expression used in rigid body dynamics. The outward inertia forces play an important role in the investigation of rail vehicle dynamics and stability during complex motion scenarios such as curve negotiations. These forces are used to define the balance speed that must be observed in order to avoid derailments during curve negotiations. The expression of the fluid outward inertia force, can be systematically derived from the inertia force as  $F_c = (m_f \ddot{\mathbf{r}}_c) \cdot \mathbf{n}$ , where  $m_f$  is the total mass of the fluid,  $\ddot{\mathbf{r}}_c$  is the acceleration of the fluid center of mass, and  $\mathbf{n}$  is the outward unit vector normal to the curve [16,17]. The position of the fluid center of mass can be derived using the moment of mass as  $\mathbf{r}_c = (\int_v \rho \mathbf{r} dv) / m_f$ .

### 5. Bulkheads/crude oil contact

The oil/tank and oil/bulkhead contact forces are formulated using a penalty approach in which the interaction forces are defined as function of the relative displacements and velocities of the bodies in contact at the contact points. The penalty formulation does not eliminate any degrees of freedom because no contact constraints are imposed on the oil, tank, and bulkhead motion. The fluid/tank interaction can also be modeled using the concept of the ANCF reference node (RN) [21]. However, the ANCF-RN approach, as compared to the penalty approach, is more restrictive since it eliminates degrees of freedom, and may lead to imposing unrealistic constraints on the motion of the fluid. Furthermore, the penalty coefficient can be adjusted to account for the fluid rheological properties. The resulting penalty-contact boundary problem is referred to as *boundary nonlinearity* [43]. In this study, the tank is treated as a rigid body, and frictionless or no-slip boundary conditions can be imposed at the rigid tank walls according to the fluid rheological properties. The penalty formulation used to define the contact forces between the oil and a cylindrical tank with half-ellipsoid ends is the same as the one used by Shi et al. [17] and Nicolsen et al. [16]. In this paper, this penalty contact formulation is extended to the case of a tank with bulkheads, used as sloshing suppression devices.

#### 5.1. Liquid sloshing suppression methods

The nonlinear dynamic effect generated by liquid sloshing is one of the most challenging problems in the rail, highway, and aerospace fluid transportation. When a fluid oscillates inside a container, it is subjected, in general, to different sources of damping: damping at the fluid/tank interface, viscous damping at the fluid free surface, internal fluid damping due to viscous forces, and damping due to the relative motion between the fluid and sloshing suppression devices, such as baffles [44]. Over the last 50 years, several analytical, experimental, and numerical methods have been developed to study the dynamic effects of liquid sloshing in moving containers. The development of analytical methods to predict liquid sloshing loads is not easy, especially if different damping forces are considered. Scarsi [45] presented analytical and experimental studies on the effect of liquid viscosity on the sloshing oscillation frequencies. Henderson and Miles [46] and Martel et al. [47] examined the dynamic characteristics of water waves in cylindrical containers and showed that the damping effect due to the fluid viscosity is negligible when the tank lateral dimension is close to the wavelength.

When the energy dissipation due to the internal fluid viscosity and the interaction with the tank walls is not sufficient to damp out the fluid hydrodynamic forces, it is recommended to divide the tank into compartments, also called *bulkheads*, or introduce other sloshing suppression devices (such as baffles, floating cans, floating lids, and sound suppressors). The advantages of these sloshing suppression devices were confirmed by Chiba et al. [48], who conducted experimental tests to study the effect of fluid viscosity. It was shown that as the tank size increases, the viscous damping effect decreases and the liquid sloshing amplitude increases. A large number of investigations were devoted to examine the effect of the liquid sloshing on tanks with different geometries and equipped with different types of baffles [49–59].

#### 5.2. Bulkhead contact forces

Accurate detection of the contact points and precise formulation of the oil/tank contact forces are necessary in order to study the dynamic interaction between the crude oil and a rail tank car equipped with bulkheads. The position of a fluid point

on an ANCF element  $j$  can be written as  $\mathbf{r}_F^j = \mathbf{S}_F^j \mathbf{e}^j$ , where  $\mathbf{S}_F^j = \mathbf{S}^j(\mathbf{x}_F)$  is the shape function matrix evaluated at point  $\mathbf{x}_F^j = [\xi_F \ \eta_F \ \zeta_F]^T$  as shown in Fig. 3, where  $\xi_F, \eta_F$ , and  $\zeta_F$  are the dimensionless spatial parameters that enter into the definition of the element shape function matrix. Fig. 4 shows a general contact configuration that will be used in the discussion presented in the remainder of this section. The global position of the tank reference point  $T$  and the orientation of the tank with respect to the global coordinate system  $XYZ$  are defined, respectively, by  $\mathbf{R}^t$  and by the transformation matrix  $\mathbf{A}^t$ . The location of a bulkhead  $i$  is defined in the tank coordinate system  $x^t y^t z^t$  as  $\mathbf{r}_B^i = [\bar{u}_{Bx}^i \ 0 \ 0]^T$ . In the global reference frame, the position of bulkhead reference point  $B^i$  is defined as  $\mathbf{r}_B^i = \mathbf{R}^t + \mathbf{b}^i$ , where  $\mathbf{b}^i = \mathbf{A}^t \bar{\mathbf{u}}_B^i$ . The relative position and velocity of the fluid boundary points with respect to bulkhead  $i$  are defined, respectively, as  $\mathbf{u}_F^{fb} = \mathbf{r}_F - \mathbf{r}_B^i$  and  $\dot{\mathbf{u}}_F^{fb} = \dot{\mathbf{r}}_F - \dot{\mathbf{r}}_B^i$ . In order to define the penetration  $\delta$  and the penetration rate  $\dot{\delta}$ , the relative position and velocity vectors  $\mathbf{u}_F^{fb}$  and  $\dot{\mathbf{u}}_F^{fb}$  must be defined in the tank body coordinate system as  $\bar{\mathbf{u}}_F^{fb} = (\mathbf{A}^t)^T \mathbf{u}_F^{fb}$  and  $\dot{\bar{\mathbf{u}}}_F^{fb} = (\mathbf{A}^t)^T (\dot{\mathbf{u}}_F^{fb} - \tilde{\omega}^t \mathbf{u}_F^{fb})$ , respectively, where  $\tilde{\omega}^t$  is the skew symmetric matrix associated with the tank angular velocity vector  $\omega^t$ . Using these definitions, the penetration and penetration rate are defined as  $\delta = (t_h/2) - \bar{u}_{Fn}^{fb}$  and  $\dot{\delta} = \dot{\bar{u}}_{Fn}^{fb} \cdot \hat{\mathbf{n}}^i$ , respectively, where  $t_h$  is the bulkhead thickness,  $\bar{u}_{Fn}^{fb} = \bar{\mathbf{u}}_F^{fb} \cdot \hat{\mathbf{n}}^i$ , and  $\hat{\mathbf{n}}^i$  is the unit vector normal to bulkhead  $i$ , as shown in Fig. 5. The magnitude of the normal and tangential contact forces are defined, respectively, as  $f_n = k_p \delta + c_p |\delta| \dot{\delta}$  and  $f_t = \mu f_n$ , where  $k_p$  and  $c_p$  are the stiffness and damping contact coefficients, and  $\mu$  is the friction coefficient at the tank and bulkheads walls [60]. In general, the penalty contact force vector at bulkhead  $i$  can be written in the global coordinates as  $\mathbf{F}_C = \mathbf{A}^t (f_n \hat{\mathbf{n}}^i - f_t \hat{\mathbf{t}}^i)$ , where  $\hat{\mathbf{t}}^i$  is a unit vector which defines the tangential direction of the local relative velocity vector  $\bar{\mathbf{v}}_t = \dot{\bar{\mathbf{u}}}_F^{fb} - (\bar{\mathbf{u}}_F^{fb} \cdot \hat{\mathbf{n}}^i) \hat{\mathbf{n}}^i$ . The virtual work of the contact forces acting on the fluid and the tank can be written as  $\delta W_C = \mathbf{F}_C^T (\delta \mathbf{r}_F - \delta \mathbf{r}_B^i)$  which can be written for an ANCF element  $j$  as  $\delta W_C = \mathbf{F}_C^T \delta \mathbf{e}^j - \mathbf{F}_C^T (\delta \mathbf{R}^t - \mathbf{A}^t \bar{\mathbf{u}}_p \bar{\mathbf{G}}^t \delta \theta^t)$  [61],  $\bar{\mathbf{G}}^t$  is the matrix that defines the relationship between the tank angular velocity  $\bar{\omega}^t$  and the time rate of the vector of rigid body orientation parameters  $\theta^t$  as  $\bar{\omega}^t = \bar{\mathbf{G}}^t \dot{\theta}^t$ , and  $\bar{\mathbf{u}}_p$  is the skew-symmetric matrix associated with vector  $\bar{\mathbf{u}}_p^t$  which defines the

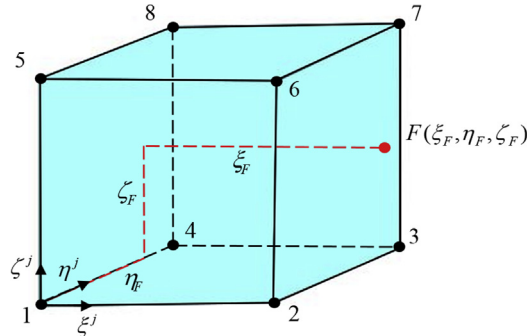


Fig. 3. Fluid point  $F$  on the outer surface of an ANCF brick element  $i$ .

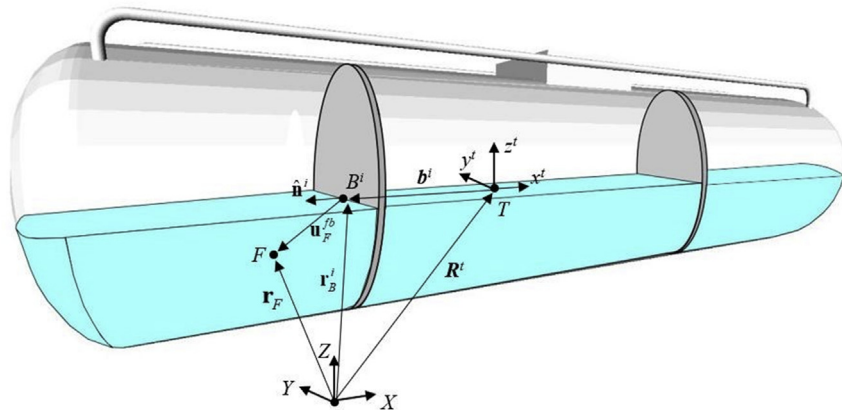


Fig. 4. Bulkheads contact.

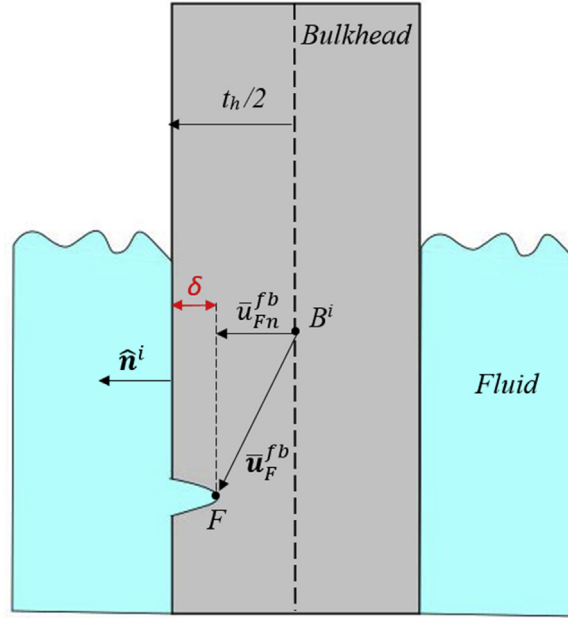


Fig. 5. Oil/bulkhead contact (penetration is magnified).

location of a tank contact point in the tank local coordinate system. The generalized forces associated with the rigid tank and with the ANCF element  $j$  nodal coordinates due to oil contact with the bulkheads can be written, respectively, as  $\mathbf{Q}_{CB}^{t^T} = -\mathbf{F}_C^T [\mathbf{I} - \mathbf{A}^t \tilde{\mathbf{u}}_p^t \mathbf{G}^t]$  and  $\mathbf{Q}_{CB}^{j^T} = \mathbf{F}_C^T \mathbf{S}^j$ . The vector of generalized fluid/tank contact forces associated with the nodal coordinates of ANCF element  $j$  can be written as  $\mathbf{Q}_C^j = \mathbf{Q}_{CB}^j + \mathbf{Q}_{CT}^j$ , where  $\mathbf{Q}_{CT}^j$  is the vector of generalized forces due to the contact between the fluid and the tank walls.

## 6. MBS equations of motion

In order to perform the nonlinear dynamic simulation of the railroad vehicle systems using MBS algorithms to examine the oil sloshing effect, the track geometry and the wheel and rail profiles are first defined at a preprocessing stage. The pre-processor produces a geometry file used as input to the main processor, which formulates and numerically solves the nonlinear dynamic equations of motion of the railroad vehicle models [60]. In this study, the rails are treated as rigid bodies, and their rigid geometry is defined using fully parameterized three-dimensional ANCF beam elements.

### 6.1. Augmented form of the equations of motion

The general equations of motion of a railroad vehicle model consisting of rigid and flexible ANCF bodies can be written in terms of the system generalized reference and ANCF nodal coordinates  $\mathbf{q}_r$  and  $\mathbf{e}$ , respectively. The geometry of the wheel and rail surfaces are defined using surface parameter  $\mathbf{s}$  that are treated as non-generalized coordinates and used to predict online the location of the wheel/rail contact points. Joint constraints and specified motion trajectories are defined using a set of nonlinear algebraic constraint equations which can be written in a vector form as  $\mathbf{C}(\mathbf{q}_r, \mathbf{e}, \mathbf{s}, t) = \mathbf{0}$ , where  $t$  is time. If an elastic contact formulation is used, the constraint equations are not function of the wheel and rail surface parameters  $\mathbf{s}$ . The nonlinear algebraic constraint equations are combined with the system differential equations of motion using the technique of Lagrange multipliers  $\lambda$ . In general, the augmented form of the equations of motion can be written as

$$\begin{bmatrix} \mathbf{M}_r & \mathbf{0} & \mathbf{0} & \mathbf{C}_{\mathbf{q}_r}^T \\ \mathbf{0} & \mathbf{M}_e & \mathbf{0} & \mathbf{C}_{\mathbf{e}}^T \\ \mathbf{0} & \mathbf{0} & \mathbf{0} & \mathbf{C}_{\mathbf{s}}^T \\ \mathbf{C}_{\mathbf{q}_r} & \mathbf{C}_{\mathbf{e}} & \mathbf{C}_{\mathbf{s}} & \mathbf{0} \end{bmatrix} \begin{bmatrix} \ddot{\mathbf{q}}_r \\ \ddot{\mathbf{e}} \\ \ddot{\mathbf{s}} \\ \lambda \end{bmatrix} = \begin{bmatrix} \mathbf{Q}_r \\ \mathbf{Q}_e \\ \mathbf{0} \\ \mathbf{Q}_d \end{bmatrix} \quad (10)$$

where  $\ddot{\mathbf{q}}_r$ ,  $\ddot{\mathbf{e}}$ , and  $\ddot{\mathbf{s}}$  are, respectively, the second time derivatives of the reference, ANCF, and non-generalized coordinates;  $\mathbf{M}_r$  and  $\mathbf{M}_e$  are, respectively, the mass matrix associated with the reference and ANCF coordinates;  $\mathbf{C}_{\mathbf{q}_r}$ ,  $\mathbf{C}_{\mathbf{e}}$ , and  $\mathbf{C}_{\mathbf{s}}$  are, respectively, the constraint Jacobian matrices resulting from the differentiation with respect to the reference, ANCF, and non-generalized

coordinates;  $\mathbf{Q}_r$  and  $\mathbf{Q}_e$  are, respectively, the vectors of generalized forces associated with the reference and ANCF nodal coordinates, and  $\mathbf{Q}_d$  is a quadratic velocity vector that results from the differentiation of the constraint equations twice with respect to time. The solution of the preceding equation defines the generalized and non-generalized accelerations as well as the vector of Lagrange multipliers  $\lambda$ , which can be used to determine the constraint forces. It is clear from the preceding equation that the non-generalized surface parameters  $\mathbf{s}$  do not have inertia or generalized forces associated with them [60,62].

## 6.2. Fluid equations of motion

The fluid (oil) partial differential equations of equilibrium are given by  $(\nabla \sigma^T)^T + \mathbf{f}_b - \rho \mathbf{a} = \mathbf{0}$ , where  $\sigma$  is the Cauchy stress tensor,  $\mathbf{f}_b$  is the vector of body forces,  $\rho$  is the mass density, and  $\mathbf{a}$  is the absolute acceleration vector. The Navier-Stokes equations, which govern the incompressible-fluid behavior, can be obtained by substituting into the partial differential equations of equilibrium the expression of the Cauchy stress tensor based on the chosen fluid constitutive model. The incompressibility condition resulting from the fluid continuity equation is reduced to  $\nabla \cdot \mathbf{v} = 0$ , where  $\mathbf{v}$  is the absolute velocity vector. Using the continuum-based Lagrangian fluid formulation discussed in this paper, the strong nonlinearity associated with the convective term of the acceleration vector  $\mathbf{a} = D\mathbf{v}(\mathbf{r}, t)/Dt = (\partial \mathbf{v}(\mathbf{r}, t)/\partial t) + \mathbf{v} \cdot \nabla \mathbf{v}$  vanishes and the acceleration can be written as a function of the material coordinates  $\mathbf{X}$  as  $\mathbf{a} = d\mathbf{v}(\mathbf{X}, t)/dt$ . Applying the principle of virtual work and using the ANCF displacement field, the partial differential equations of motion can be systematically converted to a set of discrete ordinary differential equations [21], which can be written as

$$\mathbf{M}_e^j \ddot{\mathbf{e}}^j = \mathbf{Q}_e^j \quad (11)$$

where  $\mathbf{Q}_e^j = \mathbf{Q}_b^j + \mathbf{Q}_t^j + \mathbf{Q}_c^j - \mathbf{Q}_p^j + \mathbf{Q}_v^j$ ,  $\mathbf{Q}_b^j$  and  $\mathbf{Q}_t^j$  are the vectors of generalized body and surface traction forces, respectively,  $\mathbf{Q}_c^j$  is the vector of generalized contact forces,  $\mathbf{Q}_v^j$  is the vector of generalized viscous forces,  $\mathbf{Q}_p^j$  is the vector of generalized penalty forces, and  $\mathbf{M}_e^j$  is the constant symmetric mass matrix of ANCF element  $j$ . Equation (11) can be used with a standard FE assembly procedure to define the FE mesh equations  $\mathbf{M}_e \ddot{\mathbf{e}} = \mathbf{Q}_e$ , where  $\ddot{\mathbf{e}}^j = \mathbf{B}^j \ddot{\mathbf{e}}$ ,  $\mathbf{M}_e = \sum_{j=1}^{n_e} \mathbf{B}^{jT} \mathbf{M}_e^j \mathbf{B}^j$ ,  $\mathbf{Q}_e = \sum_{j=1}^{n_e} \mathbf{B}^{jT} \mathbf{Q}_e^j$ , and  $\mathbf{B}^j$  is a Boolean matrix that defines the element connectivity.

## 7. Wheel/rail interaction

Oil sloshing can lead to oscillations in the contact forces between the wheels and rails. The variations in the contact forces as the result of the sloshing must be quantified in order to have a better understanding of the nonlinear dynamics and stability of the rail vehicles when transporting hazardous materials such as crude oils. To this end, the wheel and rail geometry and material properties that enter into the formulation of the contact forces must be accurately defined. For instance, accurate description of the wheel and rail profiles is necessary to determine the location of the contact points, define the local tangent and normal vectors, and evaluate the normal contact forces, tangential creep forces, and spin moment that have a significant effect on the railroad vehicle dynamics and stability.

### 7.1. Wheel and rail profiles

In this investigation, the wheel and rail profiles are described in a general form using differential geometry methods. The rail profile can be defined by means of three parametric equations:  $X = s_1^r$ ;  $Y = s_2^r$ ;  $Z = f(s_2^r)$ , where  $s_1^r$  is the longitudinal arc length parameter and  $s_2^r$  is the rail lateral surface parameter. In the case of a curved track, one needs also to specify the position and orientation of the rail cross section as a function of the parameter  $s_1^r$ . In railroad applications, a rail track is constructed by connecting multiple segments at nodes as described in the literature [63]. At the preprocessing stage of the computer simulation of railroad vehicles, information on each track segment must be provided, including length, curvature, super-elevation, and grade at the segment nodes.

The wheel surface can be defined by the equation  $\bar{u}(s_1, s_2) = [x_0 + g(s_1^w) \sin s_2^w \quad y_0 + s_1^w \quad z_0 - g(s_1^w) \cos s_2^w]^T$ , where  $s_1^w$  is a lateral surface parameter,  $s_2^w$  is an angular surface parameter, and  $x_0, y_0$  and  $z_0$  are the coordinates of the origin of the profile coordinate system with respect to the wheel coordinate system [60]. The wheel and rail surface parametrization is shown in Fig. 6. The wheel diameter used in this investigation is 914 mm and the profile type is AAR-1B-WF with a 1:20 taper in the tread wheel section. The rail profile is of type UIC 60.

### 7.2. Wheel/rail contact

Different approaches have been used in the literature to study the wheel/rail contact. In some approaches, the contact is treated as a two-dimensional problem while more advanced formulations impose three-dimensional contact conditions. In this paper, the wheel/rail contact problem is solved using the three-dimensional elastic contact formulation ECF-A proposed

in Ref. [62]. According to the *ECF-A* formulation, the wheel has six degrees of freedom with respect to the rail, the wheel and rail surfaces have a common normal at the contact points (non-conformal contact), and the contact force is represented by a compliant force element. The *ECF-A* method is recommended to study derailment scenarios because it allows for wheel/rail separation. As previously mentioned, the wheel/rail contact surfaces can be parametrized using the four surface parameters  $\mathbf{s} = [s_1^r \ s_2^r \ s_1^w \ s_2^w]^T$ . The location of the contact points is defined by solving the set of nonlinear algebraic equations  $\mathbf{C}(\mathbf{s}^w, \mathbf{s}^r) = [\mathbf{r}^{wr} \cdot \mathbf{t}_1^r \ \mathbf{r}^{wr} \cdot \mathbf{t}_2^r \ \mathbf{n}^r \cdot \mathbf{t}_1^w \ \mathbf{n}^r \cdot \mathbf{t}_2^w] = \mathbf{0}$ , where  $\mathbf{t}_l^k = \partial \mathbf{r}^k / \partial s_l^k$ ,  $l = 1, 2$ ;  $k = w, r$  are the tangent vectors to the surface at the contact point,  $\mathbf{n}^r = \mathbf{t}_1^r \times \mathbf{t}_2^r$  is the normal vector to the rail surface at the contact point, and  $\mathbf{r}^{wr} = \mathbf{r}^w - \mathbf{r}^r$  is the vector between the two potential contact points on the wheel and the rail. After determining the surface parameters by solving the system of nonlinear algebraic equations  $\mathbf{C}(\mathbf{s}^w, \mathbf{s}^r) = \mathbf{0}$  using a Newton-Raphson algorithm, the penetration is calculated as  $\delta = \mathbf{r}^{wr} \cdot \mathbf{n}^r$ . The normal contact force is defined according to the Hertz's contact theory with the addition of a damping component proportional to the velocity of the penetration  $\dot{\delta}$  as  $f_n = -K_h \delta^{3/2} - C \dot{\delta} |\dot{\delta}|$ , where  $K_h$  and  $C$  are the Hertzian stiffness constant and the damping coefficient, respectively. The creep forces are calculated using Kalker's USETAB routine [64,65].

## 8. Simulation results

The continuum-based total Lagrangian crude oil formulation discussed in this paper is systematically integrated with a complex MBS railroad-vehicle algorithm. Different railroad motion scenarios are investigated to study the effect of crude oil sloshing on the vehicle dynamics and stability. In this investigation, the tank is assumed partially filled with oil in order to produce significant sloshing. Partially filled tanks have the advantage of lowering the vehicle center of gravity, but result in more severe sloshing forces and oscillations. The oil inside the tank is meshed using isoparametric ANCF brick (solid) elements. Each ANCF brick element has 8 nodes and is based on an incomplete polynomial representation [66]. The ANCF brick elements ensure the continuity of the time-rate of the position vector gradients at each node. Continuity conditions can be systematically enforced to guarantee position and gradient continuity at the element interface, thus reducing the model dimensionality. A description of this element displacement field is presented in [Appendix A](#). ANCF brick elements have been successfully used in MBS truck and railroad-vehicle sloshing simulations [16,17]. Furthermore, the use of ANCF brick elements to model liquid sloshing problems has been recently validated against experimental and numerical data [67]. The sloshing

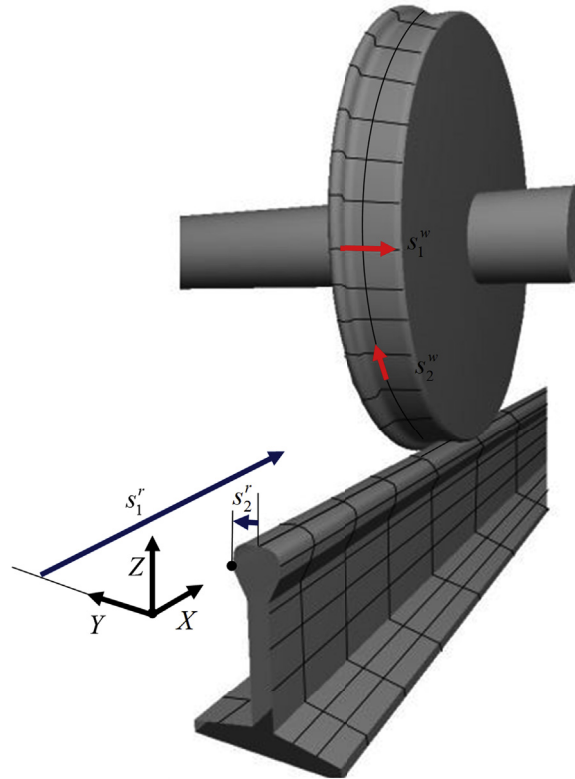


**Fig. 6.** Wheel/rail surface parameters.

**Table 1**

Curved track geometry.

Segment points No.	Distance (ft)	Curvature (Deg.)	Super-elevation (in)	Grade (%)	Right rail cant angle (rad)	Left rail cant angle (rad)
A	0	0	0	0	0.025	-0.025
B	100	0	0	0	0.025	-0.025
C	300	3	3	0	0.025	-0.025
D	600	3	3	0	0.025	-0.025
E	800	0	0	0	0.025	-0.025
F	1000	0	0	0	0.025	-0.025
G	1200	-3	-3	0	0.025	-0.025
H	1500	-3	-3	0	0.025	-0.025
I	1700	0	0	0	0.025	-0.025
J	2800	0	0	0	0.025	-0.025

**Table 2**

Crude oil rheological properties.

Crude oil type	Density (kg/m <sup>3</sup> )	Dynamic Viscosity (Pa·s)	Yield stress (Pa)
Light	850	0.005	0
Medium	900	10	30
Heavy	1000	100	100

effects produced by three different crude oils (heavy, medium, and light) are investigated in both cases of curved and straight tracks. The geometry of the curved track used in this numerical study is defined in [Table 1](#). Among the crude oil constitutive models presented in [Section 2](#), the Oldroyd type was chosen in order to avoid the numerical difficulties resulting from the use of non-physics-based rigid-solid/liquid transition model. The physical properties of the three different crude oils are shown in [Table 2](#). In the case of the braking scenario, both conventional and ECP braking systems are considered. The MBS equations of motion are integrated numerically using the implicit Hilber-Hughes-Taylor (HHT) algorithm. A reduced integration scheme is used to alleviate the volumetric locking effects.

### 8.1. Railroad MBS vehicle model

In this section, two detailed MBS railroad vehicle models used by Shi et al. [17] are considered. These models are used to demonstrate the implementation of the nonlinear ANCF crude oil sloshing formulation presented in the paper in a computational MBS railroad vehicle algorithm. The first model is a one-car railroad vehicle equipped with a cylindrical tank with half-ellipsoid ends, as shown in [Fig. 7](#). The rail car consists of two bogies, two stub sills, and one tank; each bogie includes two wheelsets, two equalizers, one frame, and one bolster. The wheelsets are connected to the frame using primary suspensions and to the equalizers using journal bearings. Each bolster is connected to the frame using a pin joint and to the stub sill by means of secondary suspensions. The stub sills are rigidly connected to the tank. The one-tank railroad vehicle model has 73 degrees of freedom. The second model is a two-car train; the two cars are connected by a coupler modeled using a linear spring-damper-actuator element, as shown in [Fig. 8](#). In both vehicle models, the tank has a length of approximately 12 m and a radius of 1.5 m. The dimensions and inertia properties of each car are the same as that presented in the literature [62].

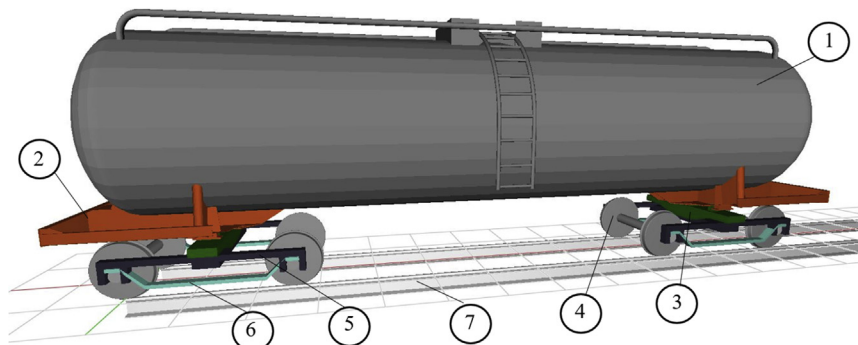


**Fig. 7.** Freight train car model. (1-Tank, 2-Stub sill, 3-Bolster, 4-Wheelset, 5-Frame, 6-Equalizer, 7-Rail).

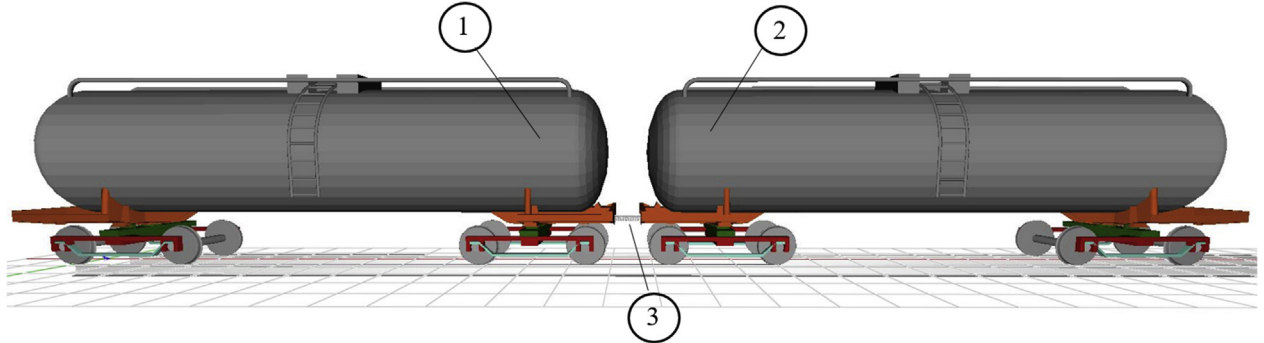


**Fig. 8.** Freight train 2-cars model. (1-Car 1, 2-Car 2, 3-Coupler).

## 8.2. ECP braking

Two braking scenarios are considered to study the effect of the crude oil sloshing on the longitudinal stability of the two-car freight train model. For this model, the stiffness and damping coefficients of the coupler are assumed to be  $k = 300$  MN/m and  $c = 200$  kNs/m, respectively. In the first case, the braking torque is applied uniformly and simultaneously to the wheels of both cars in order to simulate the ECP braking scenario. The nonlinear braking torque is designed to reduce the train velocity from 40 km/h to 5 km/h in 10 s. In the second case, referred to as the conventional braking scenario, the same braking torque is applied only to the front-car wheels. First, the mesh convergence was examined for the case of ECP braking with a tank half-filled with light crude oil, which experiences larger deformation than the medium and heavy oils. The convergence of the oil center of mass position is compared in Fig. 9 for three different oil meshes of 32, 48, and 64 ANCF solid elements (900, 1260 and 1620 degrees of freedom, respectively). By examining different curves it is evident that the three meshes lead to results which are in a good agreement. Fig. 10 shows the fluid deformed shape at different time points during braking for the case of the 48-element mesh. These results show that the ANCF total Lagrangian formulation can capture complex change in the fluid free surface geometry. In order to obtain accurate representation of the fluid deformed shape in a reasonable CPU time, the simulations for the remaining braking scenarios were performed using the 48-element mesh. To capture correctly the large oil displacement resulting from severe braking torques, the oil mesh was refined near the tank back-end as shown in Fig. 11.

## 8.3. ECP braking and coupler forces

The effect of ECP braking on the coupler force when transporting different crude oils is shown in Fig. 12. In the case of ECP braking, as the fluid viscosity increases, the magnitude of the coupler force decreases considerably. In particular, the maximum value of the coupler force in the case of heavy crude oil is approximately 30% less than that of the light oil. The fluid viscosity also influences the time required for the coupler response to reach steady state (zero force amplitude). In the case of heavy crude oil, the steady state is reached within the first 7 s of the simulation, while for the light crude oil the coupler undergoes tension and compression of non-negligible amplitude until the end of the simulation. Effective and fast damping of the coupler force oscillations is beneficial in increasing its fatigue life and wear resistance; excessive coupler forces can cause coupler failure. In the case of conventional braking, the coupler is subjected to compression force throughout the entire simulation, with an average amplitude nearly ten times higher than the ECP braking case. In this case, there are no significant differences between the coupler forces generated by the three different crude oils. Compared to ECP braking, conventional braking results in higher compressive coupler forces due to the relative motion between the two cars. Because of the high car inertia, the higher compressive forces generated during conventional braking are much larger than the liquid sloshing forces and dominate the coupler dynamics. Fig. 13 shows the longitudinal displacement of the oil center of mass in the case of the ECP and conventional braking. In both cases, the amplitude of the oil longitudinal oscillation decreases as the oil viscosity increases. The larger torque generated by the ECP braking results in higher external excitations on the tank, thus in an increased longitudinal displacement of the oil center of mass. The analysis of the numerical results shows that the oil dynamic viscosity has a significant effect on the oil sloshing in the case of braking. The longitudinal coordinate of the oil center of mass is an important indicator of the loading and unloading conditions experienced by the front and rear wheels of each car during braking. The normal load experienced by the wheels of the front car is shown in Fig. 14 for each braking scenario. The normal contact forces acting on the front wheels increase as the oil density increases. In the case of ECP braking, it is interesting to note that the value of the peak contact force for the light crude oil is nearly the same as that of the heavy crude oil. The explanation for this phenomenon is that the severe longitudinal displacement experienced by the light crude oil counter-balances the effect of its lower density and leads to higher normal loads on the front wheels. The difference between front and rear wheel normal contact forces in the case of conventional braking is nearly 40% less as compared to the ECP braking case.

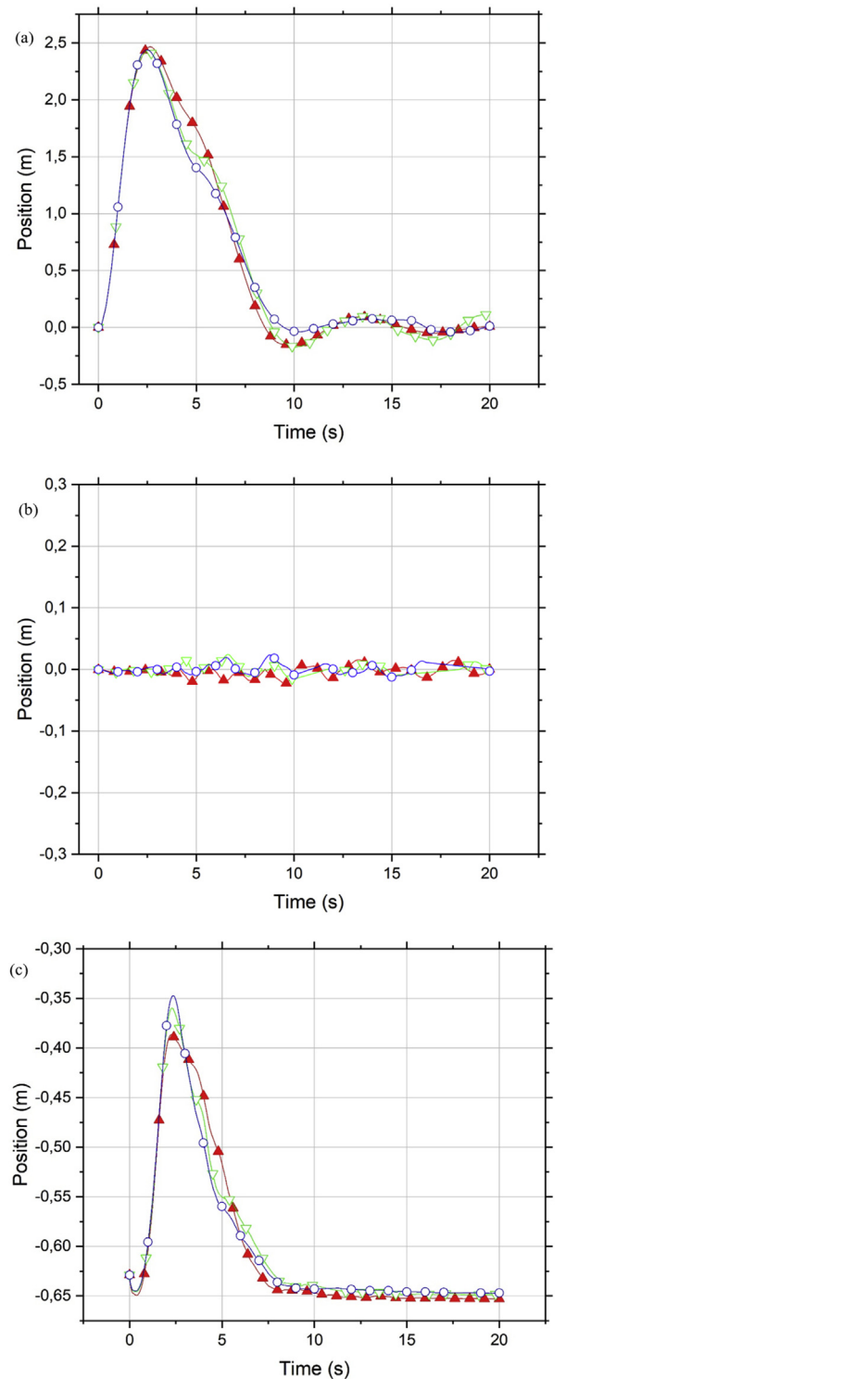


**Fig. 9.** Coordinates of the oil center of mass in the tank coordinate system. (a) X-position, (b) Y-position, (c) Z-position. (—▲— 900 DOF, —▽— 1260 DOF, —○— 1620 DOF).

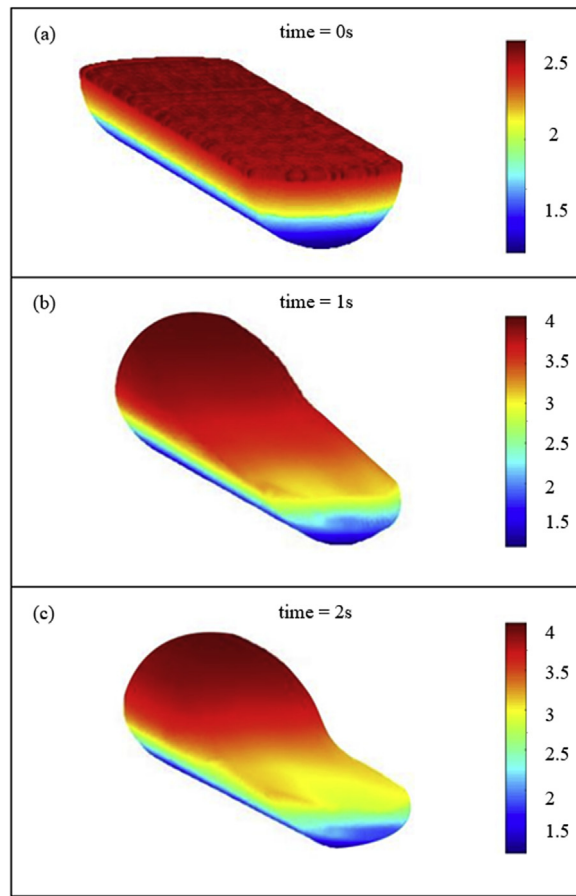


**Fig. 10.** Light crude deformed shape in time (ECP braking). Vertical liquid position is given in meter.

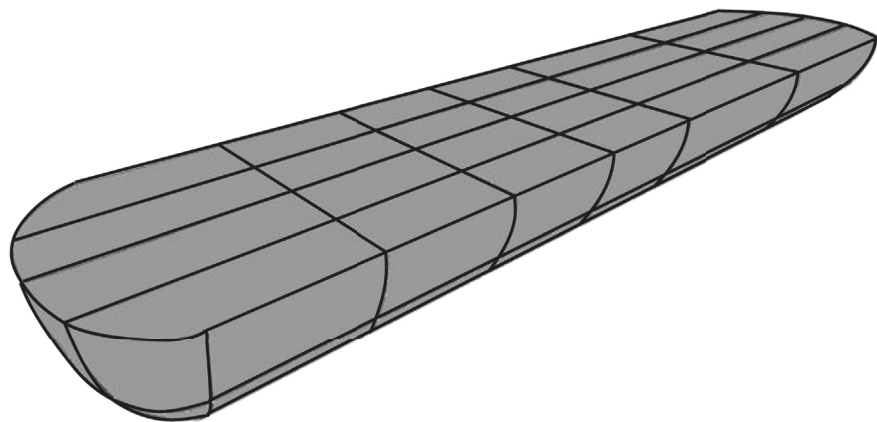


**Fig. 11.** 48-Element ANCF oil mesh.

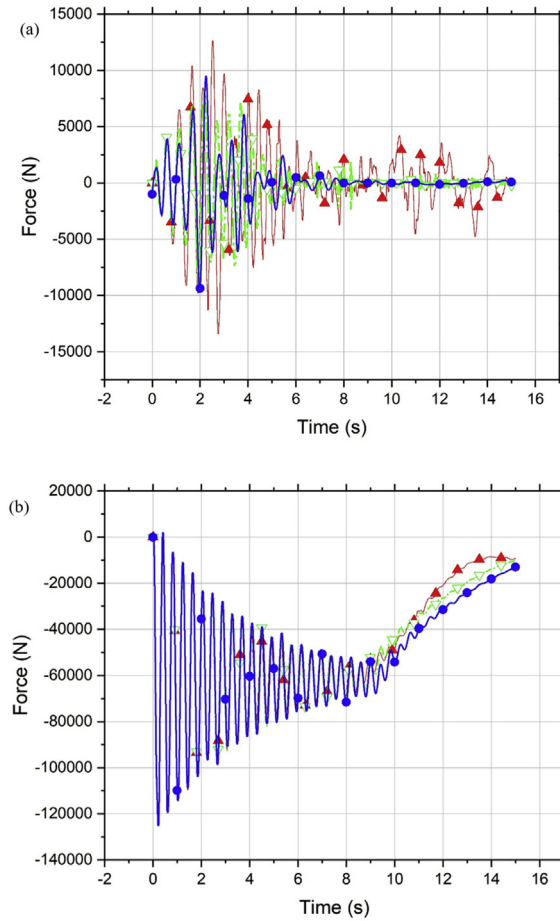


**Fig. 12.** Coupler force. (a) ECP braking, (b) Conventional braking. (—▲— Light Crude, —▽— Medium Crude, —●— Heavy Crude).

#### 8.4. Effect of using bulkheads

The simulation results already presented in this section demonstrated that the oil viscosity has a significant effect on the amplitude of the oil oscillations. However, as previously discussed in this paper, as the braking torque and tank size increase, the viscous damping effect decreases and can become almost negligible. Furthermore, the liquid sloshing loads cannot exceed certain values, defined by the design specifications, under all possible combinations of external excitations. In order to effectively control the sloshing motion and prevent vehicle instability during maneuvering, the use of sloshing suppression devices is recommended. These devices must be carefully designed to avoid the frequency of the sloshing load exciting the fundamental vibration modes of the vehicle [44]. In this section, the railroad vehicle dynamic response resulting from partitioning the tank into three compartments is examined. Fig. 15 shows the predicted coupler force in the case of ECP braking for a partitioned tank half-filled with light crude oil. The coupler force in the case of the partitioned tank is compared to the case of the same tank without bulkheads. Tank partitioning results in approximately 70% reduction of maximum coupler force and accelerates reaching its steady state, only in 5 s in this simulation scenario. The effect of the bulkheads on the wheel/rail normal contact forces is shown in Fig. 16. The resultant normal contact forces are more evenly distributed between front and rear wheels. In particular, the maximum normal force difference between front and rear wheels is reduced by nearly 60% as compared to the free tank case. These results are consistent with results previously published in the literature [68–71]. Fig. 17 compares the oil deformed shape obtained in the case of a tank with bulkheads half-filled with light crude, to the fluid shapes obtained in case of a regular tank filled with three different crude oils at time  $t = 2$  s. It is clear that a decrease in the oil viscosity results in more severe oil deformations.

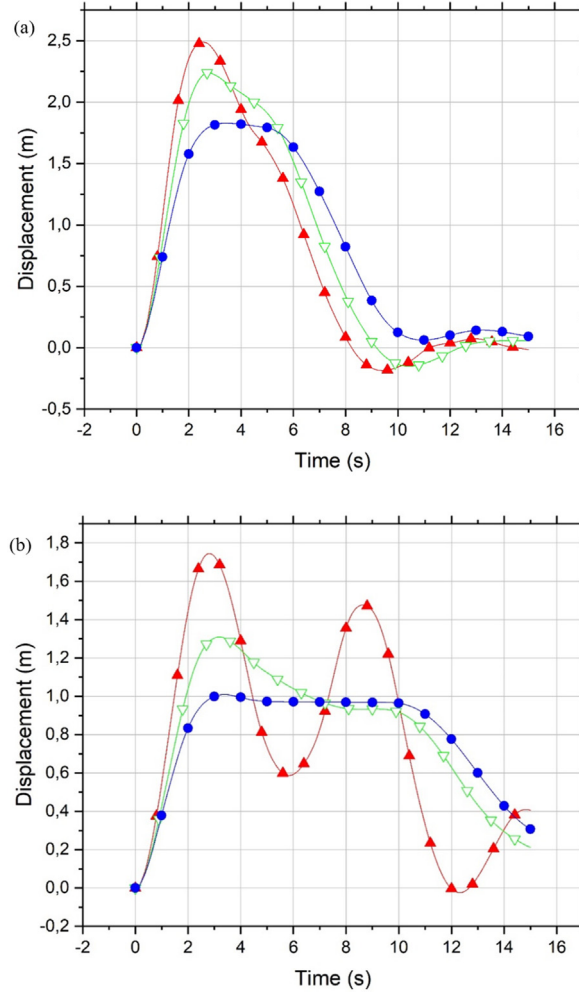


**Fig. 13.** X-displacement of the oil center of mass. (a) ECP braking, (b) Conventional braking. (—▲— Light Crude, —▽— Medium Crude, —●— Heavy Crude).

### 8.5. Curve negotiation

It is important to understand how crude oil rheological properties affect the centrifugal forces, which are the main source of instability in the case of curve negotiation. The vehicle balance speed is defined in case of rigid body dynamics as  $v = \sqrt{gRh/G}$ , where  $g$  is the gravity constant,  $R$  is the track radius of curvature,  $h$  is the super-elevation, and  $G$  is the track gage [60]. According to the data presented in Table 2 and assuming that  $R$  and  $G$  are 582 m and 1.44 m (56.685 in), respectively, the vehicle balance speed is roughly 60 km/h. In this investigation, the dynamic response of the one-car vehicle model travelling at the constant speeds of 60 km/h and 100 km/h is examined. The rail car forward velocity is defined in the MBS simulation using a trajectory coordinate constraint along the track centerline. Fig. 18 compares the value of the lateral component of the gravity force to the centrifugal force generated by each crude oil at the two different operating speeds. In general, it is observed that the oil centrifugal forces increase as a function of the density and that their amplitude decreases after the first curve due to the viscous damping. If the vehicle speed exceeds the balance speed, the oil centrifugal force becomes larger than the lateral component of gravity. In this case, the increase of the centrifugal force due to higher oil density can produce unbalance force. According to what observed in the braking scenario, crude oil viscosity has the effect of reducing the sloshing forces, including the centrifugal forces. However, even in the case of a heavy crude oil, the level of energy dissipation as the result of the oil viscosity is not sufficient to reduce the centrifugal force to a value that ensures stability, especially at velocities higher than the balance speed. As shown in Fig. 19, the wheel normal contact force increases as the crude oil density increases. At the balance speed, the centrifugal force is counterbalanced by the lateral component of gravity, and thus the super-

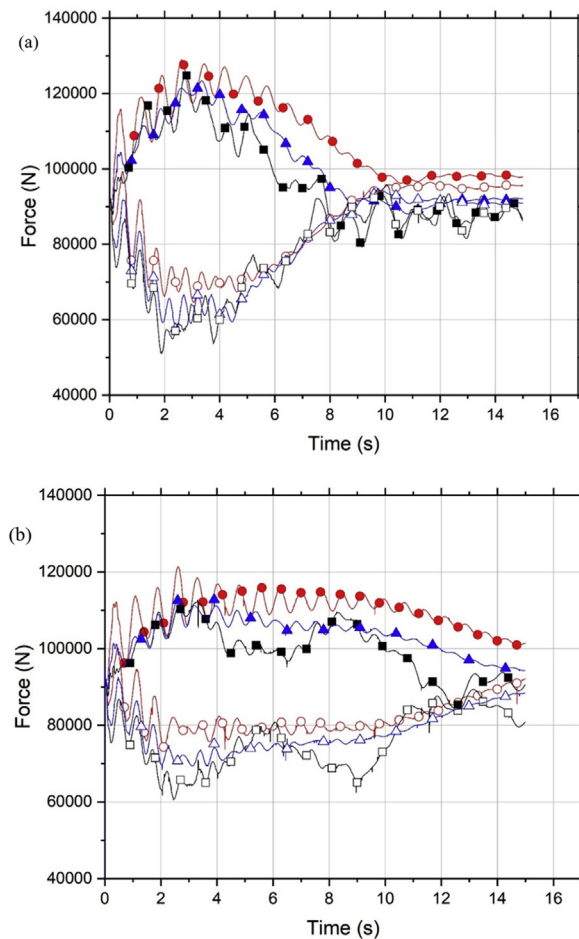


**Fig. 14.** Wheel normal contact forces. (a) ECP braking, (b) Conventional braking. (Front wheel: —■— Light Crude, —▲— Medium Crude, —●— Heavy Crude, Rear wheel: —□— Light Crude, —△— Medium Crude, —○— Heavy Crude).

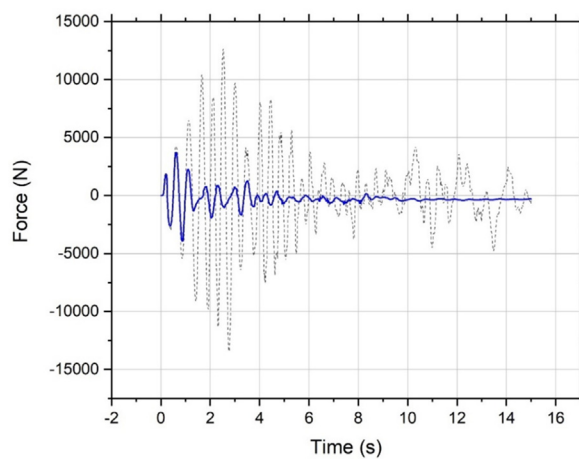


**Fig. 15.** Effect of bulkheads on the coupler force (ECP braking). (— tank with bulkheads, ----- tank without bulkheads).

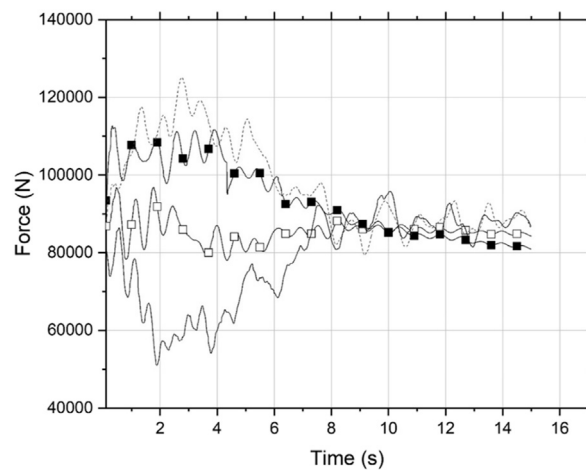


**Fig. 16.** Wheel normal contact force (ECP braking). (Front wheel: —■— tank with bulkheads, ——— tank without bulkheads, Rear wheel: —□— tank with bulkheads, ——— tank without bulkheads).

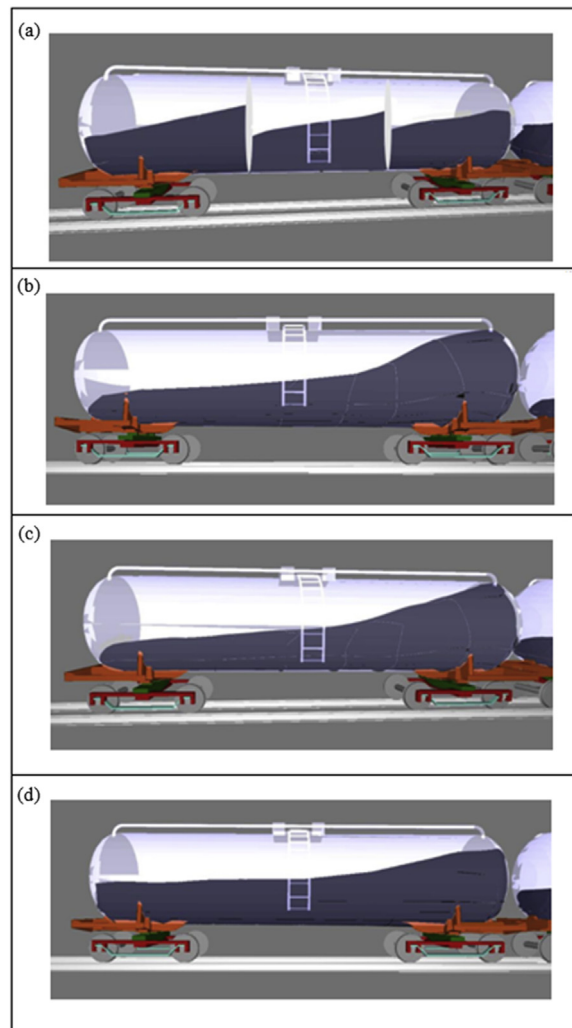


**Fig. 17.** Oil deformed shape (ECP braking at  $t = 2s$ ). (a) Bulkheads and light crude, (b) Light Crude, (c) Medium Crude, (d) Heavy Crude.

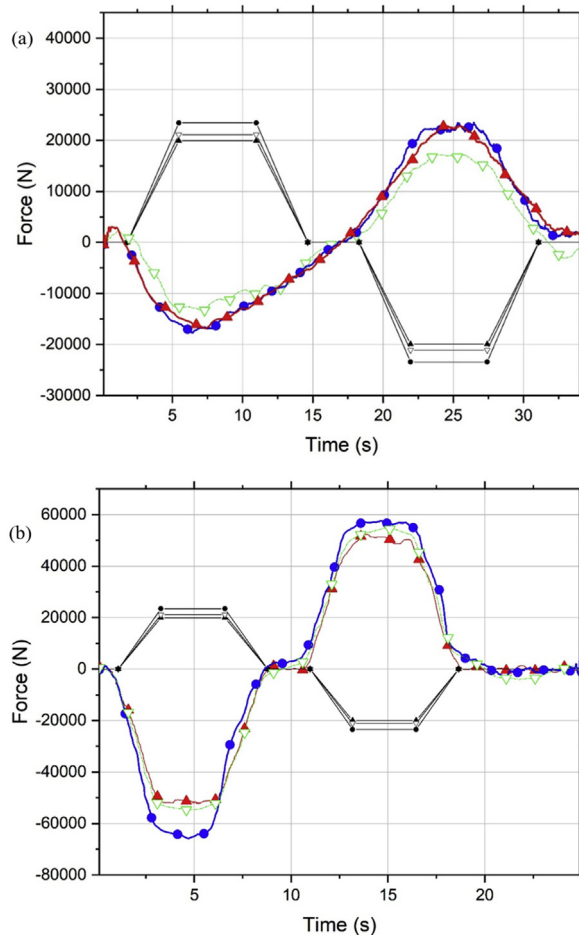


**Fig. 18.** Comparison between outward inertia force and lateral component of gravity force. (a) 60 km/h, (b) 100 km/h (—▲— Light Crude, —▽— Medium Crude, —●— Heavy Crude, —▲— Gravity LC, —▽— Gravity HC, —★— Gravity HC).

elevation leads to higher normal load on the left wheels in the first curve and on the right wheels in the second curve. However, when the train speed reaches 100 km/h and the centrifugal force is higher than the lateral component of gravity, the normal load on the right wheels becomes large in the first curve but decreases in the second curve.

## 9. Conclusions

This paper is focused on analyzing the effect of crude oil sloshing forces on railroad vehicle dynamics and stability. The continuum-based ANCF total Lagrangian formulation is used to describe accurately the oil sloshing without imposing any restriction on the amount of rotation and deformation within the finite element. The most popular crude oil constitutive models used in the literature are considered. The ANCF generalized viscous forces based on the Bingham, Herschel-Bulkley, Oldroyd and Casson constitutive models are presented. The Oldroyd constitutive model is used to examine the sloshing effect in the cases of light, medium, and heavy crude oils during different motion scenarios using two different railroad vehicle models. In the case of the ECP braking scenario, it is observed that, as the crude oil viscosity increases, and the maximum coupler force decreases approximately 30% and reaches steady state faster. In the case of conventional braking, no significant difference in the coupler forces was observed for different crude oil types. In both types of braking, it is observed that the longitudinal displacement of the oil center of mass, which serves as a good indicator of the variation of the loads on bogies

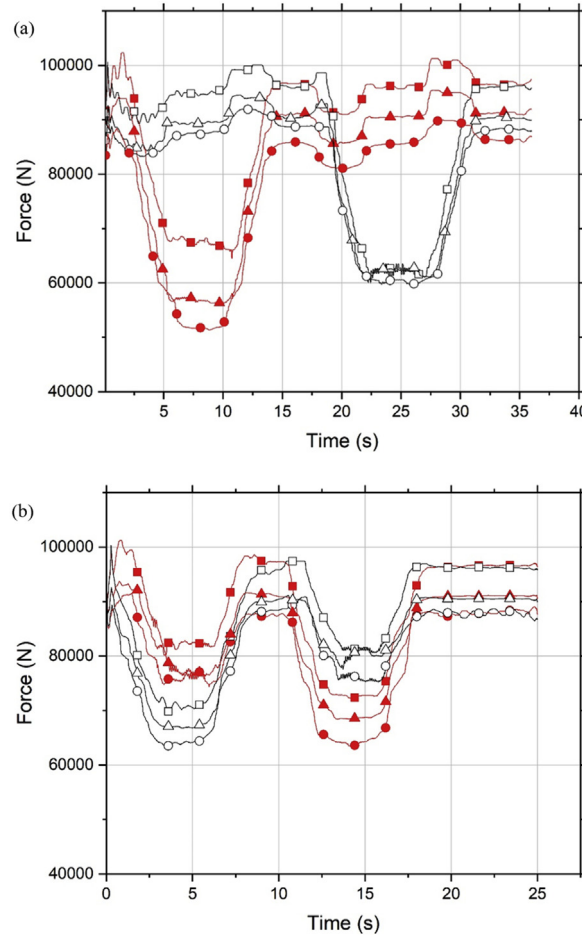


**Fig. 19.** Wheel normal contact forces in case of curved negotiation. (a) 60 km/h, (b) 100 km/h. (Right wheel: —●— Light Crude, —▲— Medium Crude, —■— Heavy Crude, Left wheel: —○— Light Crude, —△— Medium Crude, —□— Heavy Crude).

and rails, decreases as oil viscosity increases. The use of bulkheads leads to 70% reduction of the maximum coupler force, a faster decrease in amplitude of the sloshing oscillation, and a more even distribution of the normal contact forces on the front and rear wheels. In the case of curve negotiation, an increase in the oil density results in higher centrifugal forces, which can lead to unbalance force at a speed higher than the balance speed. Therefore, the oil density is an important factor in determining the oil volume in a tank.

## Acknowledgments

This research was supported by the National Science Foundation (Project # 1632302).

## Appendix A

The three-dimensional ANCF solid element, with an incomplete polynomial representation, used in this investigation is an 8-node element. The nodal coordinates  $\mathbf{e}^{jk}$  at the node  $k$  of the finite element  $j$  can be defined as

$$\mathbf{e}^{jk} = \left[ \mathbf{r}^{jk^T} \quad \mathbf{r}_x^{jk^T} \quad \mathbf{r}_y^{jk^T} \quad \mathbf{r}_z^{jk^T} \right]^T \quad k = 1, \dots, 8 \quad (\text{A. 1})$$

where  $\mathbf{r}^{jk}$  is the absolute position vector at the node  $k$  of the element  $j$ , and  $\mathbf{r}_x^{jk}$ ,  $\mathbf{r}_y^{jk}$  and  $\mathbf{r}_z^{jk}$  are the position vector gradients obtained by differentiation with respect to the spatial coordinates  $x$ ,  $y$  and  $z$ , respectively. The displacement field of each position coordinate of the solid fluid element can be defined using an incomplete polynomial with 32 coefficients as

$$\begin{aligned} \phi(x, y, z) = & \alpha_1 + \alpha_2 x + \alpha_3 y + \alpha_4 z + \alpha_5 x^2 + \alpha_6 y^2 + \alpha_7 z^2 + \alpha_8 xy + \alpha_9 yz + \alpha_{10} xz \\ & + \alpha_{11} x^3 + \alpha_{12} y^3 + \alpha_{13} z^3 + \alpha_{14} x^2 y + \alpha_{15} x^2 z + \alpha_{16} y^2 z + \alpha_{17} xy^2 + \alpha_{18} xz^2 + \alpha_{19} yz^2 \\ & + \alpha_{20} xyz + \alpha_{21} x^3 y + \alpha_{22} x^3 z + \alpha_{23} xy^3 + \alpha_{24} y^3 z + \alpha_{25} xz^3 + \alpha_{26} yz^3 + \alpha_{27} x^2 yz \\ & + \alpha_{28} xy^2 z + \alpha_{29} xyz^2 + \alpha_{30} x^3 yz + \alpha_{31} xy^3 z + \alpha_{32} xyz^3 \end{aligned} \quad (A. 2)$$

In this equation,  $\alpha_k$ ,  $k = 1, 2, \dots, 32$ , are the polynomial coefficients. Using this polynomial description, the shape functions of the ANCF brick element can be derived as follows:

$$\left. \begin{aligned} S^{k,1} &= (-1)^{1+\xi_k+\eta_k+\zeta_k} (\xi + \xi_k - 1)(\eta + \eta_k - 1)(\zeta + \zeta_k - 1) \cdot \\ & (1 + (\xi - \xi_k)(1 - 2\xi) + (\eta - \eta_k)(1 - 2\eta) + (\zeta - \zeta_k)(1 - 2\zeta)) \\ S^{k,2} &= (-1)^{\eta_k+\zeta_k} a \xi^{\xi_k+1} (\xi - 1)^{2-\xi_k} \eta^{\eta_k} (\eta - 1)^{1-\eta_k} \zeta^{\zeta_k} (\zeta - 1)^{1-\zeta_k} \\ S^{k,3} &= (-1)^{\xi_k+\zeta_k} b \xi^{\xi_k} (\xi - 1)^{1-\xi_k} \eta^{\eta_k+1} (\eta - 1)^{2-\eta_k} \zeta^{\zeta_k} (\zeta - 1)^{1-\zeta_k} \\ S^{k,4} &= (-1)^{\xi_k+\eta_k} c \xi^{\xi_k} (\xi - 1)^{1-\xi_k} \eta^{\eta_k} (\eta - 1)^{1-\eta_k} \zeta^{\zeta_k+1} (\zeta - 1)^{2-\zeta_k} \end{aligned} \right\} \quad k = 1, 2, \dots, 8 \quad (A. 3)$$

where  $a, b$ , and  $c$  are, respectively, the dimensions of the element along the axes  $x, y$ , and  $z$  directions,  $\xi = x/a$ ,  $\eta = y/b$ ,  $\zeta = z/c$ ,  $\xi, \eta, \zeta \in [0, 1]$ , and  $\xi_k, \eta_k, \zeta_k$  are the dimensionless nodal locations for node  $k$ . The position vector of an arbitrary material point on element  $j$  can be written as

$$\mathbf{r}^j = \sum_{k=1}^8 [S^{k,1} \mathbf{I} \quad S^{k,2} \mathbf{I} \quad S^{k,3} \mathbf{I} \quad S^{k,4} \mathbf{I}] \mathbf{e}^{jk} = \mathbf{S}^j \mathbf{e}^j \quad (A. 4)$$

Where  $\mathbf{I}$  is the  $3 \times 3$  identity matrix,  $\mathbf{S}^j$  and  $\mathbf{e}^j$  are, respectively, the element shape function matrix and the vector of nodal coordinates which can be written as

$$\left. \begin{aligned} \mathbf{S}^j &= [S^{1,1} \mathbf{I} \quad S^{1,2} \mathbf{I} \quad S^{1,3} \mathbf{I} \quad S^{1,4} \mathbf{I} \dots S^{8,1} \mathbf{I} \quad S^{8,2} \mathbf{I} \quad S^{8,3} \mathbf{I} \quad S^{8,4} \mathbf{I}] \\ \mathbf{e}^j &= [\mathbf{e}^{j1^T} \quad \mathbf{e}^{j2^T} \quad \mathbf{e}^{j3^T} \quad \mathbf{e}^{j4^T} \quad \mathbf{e}^{j5^T} \quad \mathbf{e}^{j6^T} \quad \mathbf{e}^{j7^T} \quad \mathbf{e}^{j8^T}]^T \end{aligned} \right\} \quad (A. 5)$$

## References

- [1] U.S. Department of Transportation, Federal Railroad Administration, Hazardous materials transportation. <https://www.fra.dot.gov/Page/P0151> (accessed 10 November 2017).
- [2] National Transportation Safety Board, Derailment of Canadian Pacific Railway Freight Train 292-16 and Subsequent Release of Anhydrous Ammonia Near Minot, North Dakota, January 18, 2002. Railroad Accident Report NTSB/RAR-04/01(2004).
- [3] King C., Trichur R., Train carrying crude oil derails in Ontario. <http://www.wsj.com/articles/train-carrying-crude-oil-derails-in-ontario-1424015961> (accessed 10 November 2017).
- [4] National Transportation Safety Board, Collision of Union Pacific Railroad Train MHOTU-23 with BNSF Railway Company Train MEAP-tul-126-d with Subsequent Derailment and Hazardous Materials Release, Macdona, Texas, June 28, 2004. Railroad Accident Report NTSB/RAR-06/03(2006).
- [5] National Transportation Safety Board, Collision of Norfolk Southern Freight Train 192 with Standing Norfolk Southern Local Train P22 with Subsequent Hazardous Materials Release at Graniteville, South Carolina, January 6, 2005. Railroad Accident Report NTSB/RAR-05/04(2005).
- [6] Holmes E., Podesta L., Cleanup underway after train carrying crude oil derails in Plainfield. <http://abc7chicago.com/news/cleanup-underway-after-train-carrying-crude-oil-derails-in-plainfield/2170862/> (accessed 10 November 2017).
- [7] D.Y. Jeong, M.L. Lyons, O. Orringer, A.B. Perlman, Equations of motion for train derailment dynamics, in: Proceedings of the 2007 ASME Rail Transportation Division Fall Technical Conference, 2007, pp. 11–12.
- [8] D.C. Tyrell, D.Y. Jeong, K. Jacobsen, E. Martinez, Improved tank car safety research, in: Proceedings of the 2007 ASME Rail Transportation Division Fall Technical Conference, 2007, pp. 11–12.
- [9] S. Rakheja, R. Ranganathan, Estimation of the rollover threshold of heavy vehicles carrying liquid cargo: a simplified approach, Int. J. Heavy Veh. Syst. 1 (1993) 79–98.
- [10] M.I. Salem, Rollover Stability of Partially Filled Heavy-duty Elliptical Tankers Using Trammel Pendulums to Simulate Fluid Sloshing, PhD thesis, West Virginia University, 2002.
- [11] D. Younesian, M. Abedi, I. Hazrati Ashtiani, Dynamic analysis of a partially filled tanker train travelling on a curved track, Int. J. Heavy Veh. Syst. 17 (2010) 331–358.
- [12] E. Di Gialetta, A. Premoli, S. Gallazzi, S. Bruni, Sloshing effects and running safety in railway freight vehicles, Veh. Syst. Dyn. 51 (2013) 1640–1654.
- [13] W. Hu, Q. Tian, H.Y. Hu, Dynamic simulation of liquid-filled flexible multibody systems via absolute nodal coordinate formulation and SPH method, Nonlinear Dynam. 75 (2014) 653–671.
- [14] C. Ma, M. Oka, T. Ando, N. Matsubara, A study on sloshing behavior for moss type LNG tank based on SPH numerical simulation and large-scale model experiment, in: The 27th International Ocean and Polar Engineering Conference, 2017.
- [15] C. Wei, L. Wang, A.A. Shabana, A total Lagrangian ANCF liquid sloshing approach for multibody system applications, J. Comput. Nonlinear Dynam. 10 (2015) 051014.
- [16] B. Nicolsen, L. Wang, A.A. Shabana, Nonlinear finite element analysis of liquid sloshing in complex vehicle motion scenarios, J. Sound Vib. 405 (2017) 208–233.
- [17] H. Shi, L. Wang, B. Nicolsen, A.A. Shabana, Integration of geometry and analysis for the study of liquid sloshing in railroad vehicle dynamics, Proc. Inst. Mech. Eng. Part K J. Multi-Body Dyn. (2017), 1464419317696418.
- [18] I. Frigaard, G. Vinay, A. Wachs, Compressible displacement of waxy crude oils in long pipeline startup flows, J. Non-Newtonian Fluid Mech. 147 (2007) 45–64.
- [19] H. Teng, J. Zhang, A new thixotropic model for waxy crude, Rheol. Acta 52 (2013) 903–911.
- [20] C. Chang, D.V. Boger, Q.D. Nguyen, The yielding of waxy crude oils, Ind. Eng. Chem. Res. 37 (1998) 1551–1559.

- [21] A.A. Shabana, Computational Continuum Mechanics, third ed., John Wiley & Sons, 2018.
- [22] C.J. Dimitriou, G.H. McKinley, R. Venkatesan, Rheo-PIV analysis of the yielding and flow of model waxy crude oils, *Energy Fuels* 25 (2011) 3040–3052.
- [23] G. Vinay, A. Wachs, J.F. Agassant, Numerical simulation of non-isothermal viscoplastic waxy crude oil flows, *J. Non-Newtonian Fluid Mech.* 128 (2005) 144–162.
- [24] S. Livescu, Mathematical modeling of thixotropic drilling mud and crude oil flow in wells and pipelines - a review, *J. Petrol. Sci. Eng.* 98 (2012) 174–184.
- [25] T. Schwerdoff, La rigidité des fluids, *Rapports du Congrès intern. de Physique* 1 (1900) 478–486.
- [26] E.C. Bingham, *Fluid and Plasticity*, McGraw-Hill, 1922.
- [27] W.H. Herschel, R. Bulkley, Measurement of consistency as applied to rubber-benzene solutions, *Am. Soc. Test Proc.* 26 (1926) 621–633.
- [28] K.V. Hohenemser, W. Prager, Über die ansätze der mechanik isotroper kontinua, *ZAMM-J. Appl. Math. Mech./Zeitschrift für Angewandte Mathematik und Mechanik* 12 (1932) 216–226.
- [29] J.G. Oldroyd, A rational formulation of the equations of plastic flow for a Bingham solid, in: *Mathematical Proceedings of the Cambridge Philosophical Society*, vol. 43, 1947, pp. 100–105.
- [30] P. Saramito, A new constitutive equation for elastoviscoplastic fluid flows, *J. Non-Newtonian Fluid Mech.* 145 (2007) 1–14.
- [31] P. Saramito, A new elastoviscoplastic model based on the Herschel–Bulkley viscoplastic model, *J. Non-Newtonian Fluid Mech.* 158 (2009) 154–161.
- [32] D.C. Cheng, F. Evans, Phenomenological characterization of the rheological behaviour of inelastic reversible thixotropic and antithixotropic fluids, *Br. J. Appl. Phys.* 16 (1965) 1599.
- [33] J. Billingham, J.W.J. Ferguson, Laminar unidirectional flow of a thixotropic fluid in a circular pipe, *J. Non-Newtonian Fluid Mech.* 47 (1993) 21–55.
- [34] H.A. Barnes, Thixotropy - a review, *J. Non-Newtonian Fluid Mech.* 70 (1997) 1–33.
- [35] A. Mujumdar, A.N. Beris, A.B. Metzner, Transient phenomena in thixotropic systems, *J. Non-Newtonian Fluid Mech.* 102 (2002) 157–178.
- [36] A. Wachs, G. Vinay, I. Frigaard, A 1.5 D numerical model for the start-up of weakly compressible flow of a viscoplastic and thixotropic fluid in pipelines, *J. Non-Newtonian Fluid Mech.* 159 (2009) 81–94.
- [37] S. Livescu, R.V. Roy, L.W. Schwartz, Leveling of thixotropic liquids, *J. Non-Newtonian Fluid Mech.* 166 (2011) 395–403.
- [38] C. Chang, Q.D. Nguyen, H.P. Rønningse, Isothermal start-up of pipeline transporting waxy crude oil, *J. Non-Newtonian Fluid Mech.* 87 (1999) 127–154.
- [39] H.T. Huynh, N. Roussel, P. Coussot, Aging and free surface flow of a thixotropic fluid, *Phys. Fluid.* 17 (2005), 033101.
- [40] B. Herhaft, A. Ragouilliaux, P. Coussot, How to unify low-shear-rate rheology and gel properties of drilling muds: a transient rheological and structural model for complex wells applications, in: *IADC/SPE Drilling Conference* Society of Petroleum Engineers, 2006.
- [41] W. Liu, K.Q. Zhu, A study of start-up flow of thixotropic fluids including inertia effects on an inclined plane, *Phys. Fluids* 23 (2011) 013103.
- [42] R.R. Huilgol, Z. You, Application of the augmented Lagrangian method to steady pipe flows of Bingham, Casson and Herschel–Bulkley fluids, *J. Non-Newtonian Fluid Mech.* 128 (2005) 126–143.
- [43] N.H. Kim, *Introduction to Nonlinear Finite Element Analysis*, Springer Science &Business Media, New York, 2014.
- [44] R.A. Ibrahim, *Liquid Sloshing Dynamics: Theory and Applications*, Cambridge University Press, 2005.
- [45] G. Scarsi, Natural frequencies of viscous liquids in rectangular tanks, *Meccanica* 6 (1971) 223–234.
- [46] D.M. Henderson, J.W. Miles, Surface-wave damping in a circular cylinder with a fixed contact-line, *J. Fluid Mech.* 275 (1994) 285–299.
- [47] C. Martel, J.A. Nicolas, J.M. Vega, Surface-wave damping in a brimful circular cylinder, *J. Fluid Mech.* 360 (1998) 213–228.
- [48] T. Chiba, S. Nakajima, T. Mieda, N. Ogawa, H. Shibata, The sloshing behavior of high viscous liquid in cylindrical tanks, in: *fluid-sloshing and fluid-structure Interaction*, in: *ASME Press Vess Piping Conf. PVP*, vol. 314, 1995, pp. 57–82.
- [49] A. Gedikli, M.E. Ergüven, Seismic analysis of a liquid storage tank with a baffle, *J. Sound Vib.* 223 (1999) 141–155.
- [50] J.R. Cho, H.W. Lee, Numerical study on liquid sloshing in baffled tank by nonlinear finite element method, *Comput. Meth. Appl. Mech. Eng.* 193 (2004) 2581–2598.
- [51] J.R. Cho, H.W. Lee, S.Y. Ha, Finite element analysis of resonant sloshing response in 2-D baffled tank, *J. Sound Vib.* 288 (2005) 829–845.
- [52] D. Liu, P. Lin, Three-dimensional liquid sloshing in a tank with baffles, *Ocean. Eng.* 36 (2009) 202–212.
- [53] P.K. Panigrahy, U.K. Saha, D. Maity, Experimental studies on sloshing behavior due to horizontal movement of liquids in baffled tanks, *Ocean Eng.* 36 (2009) 213–222.
- [54] H. Akyildiz, A numerical study of the effects of the vertical baffle on liquid sloshing in two-dimensional rectangular tank, *J. Sound Vib.* 331 (2012) 41–52.
- [55] W. Wang, Z. Guo, Y. Peng, Q. Zhang, A numerical study of the effects of the t-shaped baffles on liquid sloshing in horizontal elliptical tanks, *Ocean Eng.* 111 (2016) 543–568.
- [56] H.Q. Yang, J. West, J. Brodnick, C. Eberhart, Development of Semi-empirical Damping Equation for Baffled Tank with Oblate Spheroidal Dome, 2016.
- [57] M.A. Xue, J. Zheng, P. Lin, Z. Yuan X, Experimental study on vertical baffles of different configurations in suppressing sloshing pressure, *Ocean Eng.* 136 (2017) 178–189.
- [58] N. Thuvanismail, D.J. Surahonne, A.P. Shah, S.S. Annamalaisamy, Effect of porous baffle on sloshing pressure distribution in a barge mounted container subjected to wave excitation, in: *ASME 2017 36th International Conference on Ocean, Offshore and Arctic Engineering*, 2017. V001T01A045–V001T01A045.
- [59] Q.Y. Wang, S. Rakheja, W.B. Shangguan, Effect of baffle geometry and air pressure on transient fluid slosh in partially filled tanks, *Int. J. Heavy Veh. Syst.* 24 (2017) 378–401.
- [60] A.A. Shabana, K.E. Zaazaa, H. Sugiyama, *Railroad Vehicle Dynamics: a Computational Approach*, Taylor & Francis/CRC, Boca Raton, 2008.
- [61] A.A. Shabana, *Dynamics of Multibody Systems*, fourth ed., Cambridge University Press, Oxford, England, 2013.
- [62] A.A. Shabana, M. Tobaa, H. Sugiyama, K. Zaazaa, On the computer formulations of the wheel/rail contact problem, *Nonlinear Dynam.* 40 (2005) 169–193.
- [63] M. Berzeri, J.R. Sany, A.A. Shabana, Curved Track Modeling Using the Absolute Nodal Coordinate Formulation, Technical Report # MBS00-4-UIC, Department of Mechanical Engineering, University of Illinois, Chicago, 2000.
- [64] J.J. Kalker, K.L. Johnson, Three-dimensional elastic bodies in rolling contact, *J. Appl. Mech.* 60 (1993) 255.
- [65] J.J. Kalker, Wheel-rail rolling contact theory, *Wear* 144 (1991) 243–261.
- [66] A. Olshevskiy, O. Dmitrochenko, C.W. Kim, Three-dimensional solid brick element using slopes in the absolute nodal coordinate formulation, *J. Comput. Nonlinear Dynam.* 9 (2014), 021001.
- [67] E. Grossi, A.A. Shabana, Validation of a total Lagrangian ANCF solution procedure for fluid-structure interaction problems, *J. Verif. Validation Uncertain. Quantification* 2 (2017), 041001–1–041001–13.
- [68] F. Yang, G. Yan, S. Rakheja, Anti-slosh effectiveness of baffles and braking performance of a partly-filled tank truck, *Appl. Mech. Mater.* 541 (2014) 674–683.
- [69] J.H. Jung, H.S. Yoon, C.Y. Lee, S.C. Shin, Effect of the vertical baffle height on the liquid sloshing in a three-dimensional rectangular tank, *Ocean Eng.* 44 (2012) 79–89.
- [70] T. Kandasamy, S. Rakheja, A.K.W. Ahmed, An analysis of baffles designs for limiting fluid slosh in partly filled tank trucks, *Open Transport. J.* 4 (2010) 23–32.
- [71] G. Yan, S. Rakheja, Straight-line braking dynamic analysis of a partly filled baffled and unbaffled tank truck, *Proc. Inst. Mech. Eng. - Part D J. Automob. Eng.* 223 (2009) 11–26.